

WORKING TITLE:

Quanteneffekte, Wasser auf Metalloxidoberflächen

Dissertation zur Erlangung des akademischen Grades
›doctor rerum naturalium‹ (Dr. rer. nat.)
in der Wissenschaftsdisziplin Theoretische Chemie

vorgelegt von
Sophia L. Heiden

an der
Mathematisch-Naturwissenschaftlichen Fakultät
der Universität Potsdam



Potsdam, xx 2018

This work has been done between January 2015 and xx 2018 in the workgroup of Prof. Dr. Peter Saalfrank at the Institute of Chemistry at the University of Potsdam.

Potsdam, xx 2018

Erstgutachter: Prof. Dr. Peter Saalfrank (Uni Potsdam)
Zweitgutachter: Prof. Dr. Beate Paulus (FU Berlin)
Drittgutachter: Prof. Dr. xy

Preamble

The importance of surface science in our industrialized world is overwhelming, because most processes in industry need (heterogeneous) catalysts, because these do not have to be separated from the reactants and the product after the process, which is mostly a costly step in the production of chemicals. It is therefore desirable to understand heterogeneous catalytic processes by learning more about the processes that take place on the surface of materials. Metal oxide materials are frequently used in catalysts as well as catalyst support materials, so that understanding their properties in contact with chemicals, in this work water, is crucial.

Aluminum is used in rocket fuels as a reduction agent so that during launch alumina particles are ejected in the atmosphere during the start (see also lit.dat!). For a space shuttle the start can produce around 760,000 kg of alumina particles. It can be measured that approximately one third of these particles can be deposited in the stratosphere (in an altitude between 15 and 50 km above the surface of the earth) and there it can react with the water and other molecules in the stratosphere where these particles are accumulated after the launch of a shuttle.

Also in geochemical sciences Al_2O_3 is a subject of a variety of studies since aluminum is the third most common element in the crust with 6.3% (

http://www.unterra.de/rutherford/tab_hauf.htm

Riedel [?]: Alumina is the most abundant metal in the crust and the third most element therein. Component of feldspar, Glimmer and clay minerals (with silicates), more seldomly as corundum and "Schmirgel". Some of them are precious stones ruby, saphir

Dtv-Atlas [?]: third most abundant element, 8.1% of the earth crust and with that the far most abundant metal) and it also can be seen as a model systems for more complex aluminosilicates. Oxide rocks are omnipresent in the crust of the earth and henceforth in most geochemical processes since the times the earth's atmosphere became oxidizing with rise of photosynthetic life forms/(bacteria?) a few million years ago. Before under reductive conditions sulfidic rocks were dominant but when photosynthesis became more common with the rise of more advanced life forms, the oxygen content of the atmosphere grew.

Contents

| | |
|---|-----------|
| Preamble | 3 |
| 1 Theory und Methodology | 7 |
| 1.1 DFT | 7 |
| 1.2 Periodic Boundary Conditions | 8 |
| 1.3 Atom Centered Basis and Peculiarities | 9 |
| 1.4 Ab-initio Molecular Dynamics | 9 |
| 1.5 Frequencies and Intensities | 9 |
| 1.6 Finding Transition States | 10 |
| 1.7 From Density Functionals to Hybrids and Perturbation Theory | 11 |
| 1.8 Computational Details and Used Programs | 11 |
| 1.9 Experimental Techniques | 12 |
| 1.9.1 Vibrational Sum Frequency Generation | 12 |
| 1.9.2 Thermal Desorption Spectroscopy | 12 |
| 1.9.3 Molecular Beam Source vs. Pinhole Dosing | 12 |
| 1.9.4 Low-Energy Electron Diffraction | 13 |
| 2 Water on $\alpha\text{-Al}_2\text{O}_3(11\bar{2}0)$ | 15 |
| 2.1 Surface Model | 15 |
| 2.2 Structure Search | 17 |
| 2.3 Reactions and Microkinetic Model | 21 |
| 2.4 Vibrational Frequencies / Spectroscopic Properties | 27 |
| 2.4.1 Normal Mode Analysis | 28 |
| 2.4.2 Velocity-Velocity Autocorrelation Function | 31 |
| 2.5 Desorption Process | 31 |
| 3 Water on $\alpha\text{-Al}_2\text{O}_3(0001)$ | 33 |
| 3.1 Surface Model and Static Calculations | 33 |
| 3.2 AIMD for MBS Process | 35 |
| 3.2.1 Beam Model | 36 |

Contents

| | | |
|-------------------|--|-----------|
| 3.2.2 | Example Trajectories | 37 |
| 3.2.3 | Microcanonical AIMD at clean surface | 38 |
| 3.2.4 | Thermalized Surface | 42 |
| 3.2.5 | Refined Surface Model | 42 |
| 3.2.6 | Refined Beam Model | 42 |
| 3.3 | Improvement of Reaction Rates | 44 |
| 3.3.1 | MP2 and B3LYP | 44 |
| 3.3.2 | PIMD | 45 |
| 3.3.3 | QM/QM Embedding Scheme | 45 |
| Summary | | 47 |
| Appendix | | 49 |
| References | | 53 |

1 Theory und Methodology

In this chapter the basics of the applied theoretical methods shall be explained.

1.1 DFT

basic idea of DFT, only 3 dimensional system instead of $3N$ -dimensional with N being the number of electrons, Kohn-Sham DFT use orbitals again, methods and algorithms known from wave function based methods can be applied, functionals difference pure density functionals and hybrid, some exact exchange from Hartree Fock is mixed into the potential, functionals like B3LYP, HSE06. Dispersion corrections that account for van-der-Waals interactions, and are important for the adsorbate-surface interaction and the adsorbate-adsorbate interaction.

A test system with non-interacting electrons that reflects the systems electron density, is set and calculated.

Hohenberg-Kohn theorem connect the Hamiltonian of a many-particle system to its ground-state density $n(\underline{\mathbf{r}})$. If $\Psi(\underline{\mathbf{r}}^N)$ is an N -electron wavefunction, then the electron density can be given as

$$n(\underline{\mathbf{r}}) = N \int \dots \int \Psi^*(\underline{\mathbf{r}}, \underline{\mathbf{r}}_2, \underline{\mathbf{r}}_3, \dots, \underline{\mathbf{r}}_N) \Psi(\underline{\mathbf{r}}, \underline{\mathbf{r}}_2, \underline{\mathbf{r}}_3, \dots, \underline{\mathbf{r}}_N) d\underline{\mathbf{r}}_2 \dots d\underline{\mathbf{r}}_N \quad (1.1)$$

with Hohenberg-Kohn Theorem I the total energy $E[n]$ can be determined as:

$$E[n] = T[n] + V_{ext}[n] + V_{ee}[n] = \int n(\underline{\mathbf{r}}) v_{ext}(\underline{\mathbf{r}}) d\underline{\mathbf{r}} + T[n] + E_H[n] + E_{xc}[n] \quad (1.2)$$

with the kinetic energy $T[n]$, the potential energy $V[n]$ for electron electron interaction ee and external potential ext , the Hartree energy $E_H[n]$, corresponding to the classical Coulomb interaction and the exchange correlation energy $E_{xc}[n]$ for the non-classical exchange correlation interactions.

A problem is, that the explicit form of the interacting kinetic energy $T[n]$ and the exchange correlation functional $E_{xc}[n]$ are unknown.

1.2 Periodic Boundary Conditions

plane wave basis, no atom centered basis functions, periodic boundary conditions, electron density has to be the same in each repeating unit, Miller Indices for nomenclature of surface sites/faces (3 and 4 numbers) (hkl , $hk-(h+k)l$), how to understand these numbers, hexagonal cells, lattice types, differences between these types, Bravais lattice, Brillouin zone, \underline{k} -points, irreducible \underline{k} -points necessary for describing the system, direct and reciprocal room, how to convert between these two with the lattice vectors

Surface simulation, 2-D system reproduced as 3-D structure since vasp is bulk code there have to be 3 dimensions, so one has to define a vacuum gap between two slabs along the z-axis (perpendicular to the surface) to prevent unit cells from influencing each other and therefore lead to unphysical behaviour. Some programs (here used crystal and cp2k(?)) deliver opportunity to calculate only 2D system, repeating the slab only in x/y, a/b, respectively.

The systems are modelled as periodic solid, this can be described by a unit cell, that is translated along every spatial direction. The lattice can be described by the lattice vector \underline{B} . \underline{a}_i are basis vectors of the lattice and n_i integers:

$$\underline{B} = n_1 \underline{a}_1 + n_2 \underline{a}_2 + n_3 \underline{a}_3 \quad (1.3)$$

Analogue to that, also a reciprocal space exists (\underline{k} -space) with a set of vectors \underline{G} :

$$\underline{G} = h \underline{b}_1 + k \underline{b}_2 + l \underline{b}_3 \quad (1.4)$$

that span the lattice space. For the reciprocal space we have:

$$e^{i\underline{G}\cdot\underline{B}} = 1. \quad (1.5)$$

The unit cell within the reciprocal space is called Wigner-Seitz cell and is also referred to as first Brillouin zone, whose center is the Γ -point ($h = k = l = 0$). Between the vectors of the direct and the reciprocal space there are fixed relations and they are perpendicular to each other:

$$\underline{a}_i \cdot \underline{b}_j = 2\pi\delta_{ij}. \quad (1.6)$$

To describe periodic systems with quantum mechanical methods, one has to introduce periodic boundary conditions. These assume that the effective potential v_{eff} has to be the same in all cells that are given by \underline{B} :

$$v_{eff}(\underline{r}) = v_{eff}(\underline{r} + \underline{B}). \quad (1.7)$$

1.3 Atom Centered Basis and Peculiarities

Problem of plane waves for necessity of atom centered bases; Whenever there are atom centered basis sets the orbitals can overlap and due to this electrons are considered multiple times. This is called Basis Set Superposition Error (BSSE). One can apply Counterpoise corrections to get rid of this source of error. This is done here by calculating ghosted calculations with the system as a whole, the adsorbate alone, and the adsorbate with surface from ghost atoms. Then one applies a subtractive scheme to cancel out the effect of the orbital overlap. On the other hand one can use a huge basis set, that doesn't have this problem, which comes with a higher computational demand.

1.4 Ab-initio Molecular Dynamics

Microcanonical and Canonical ensemble, also called NVT and NVE. Difference between the two, N number of (?), V volume of the cell, T temperature and E energy; are kept constant. theory behind, calcuation of time propagation with Verlet algorithm, time steps chosen so that we don't miss the fastest processes, forces acting on atoms, Nosé Hoover thermostat.

Solve Newton's equations of motion, in principle $F = m \cdot a$ for force acting on each atom, classical ansatz.

$$-\frac{\partial V(\mathbf{R})}{\partial \underline{\mathbf{R}}(t)} = M_A \frac{d^2 \mathbf{R}_A(t)}{dt^2} \quad (1.8)$$

1.5 Frequencies and Intensities

Normal Mode Analysis, diagonalization of the Hessian, eigenvalues are frequencies squared. While this is a good approximation for the high energy vibration, for example OD stretch vibrations, it becomes worse for lattice vibrations, which are way more delocalized. A characteristic of stationary points on the potential energy surface is, that the derivation with respect to all coordinates equals 0. For these points (minima and saddle points of first order) the Hessian matrix and their eigenvalues are of interest. The elements of this Hessian are the derivation of the potential with respect to coordinates:

$$H_{ij} = \left(\frac{\partial^2 V}{\partial Q_i \partial Q_j} \right)_{|Q_i=Q_j=0} = \left(\frac{1}{\sqrt{m_i m_j}} \frac{\partial^2 V}{\partial R_i \partial R_j} \right) \quad (1.9)$$

1 Theory und Methodology

Here, Q_i are mass weighted coordinates $Q_i = \sqrt{m_i}R_i$, with the mass m_i and the displacement from the equilibrium position R_i . Then the matrix problem for the Hessian $\underline{\underline{H}}$ has to be solved:

$$\underline{\underline{H}} \underline{\underline{A}}_i = \lambda_i \underline{\underline{A}}_i. \quad (1.10)$$

with the vectors of the normal modes A_i and λ_i being the squares of vibrational frequencies ω_i :

$$\omega_i = \sqrt{\lambda_i}. \quad (1.11)$$

One has to distinguish two physically relevant cases: all eigenvalues are positive ($\lambda_i \geq 0 \forall i$) so the structure is a minimum on the PES. This could be the educt and product of a reaction. The second relevant case is if there is only one negative eigenvalue, that gives according to equation 1.11 one imaginary frequency, respectively. This is in a mathematical sense a saddlepoint of first order and can be interpreted as a transition state.

dipole corrected NMA intensity can be calculated for IR spectra, not the same selection rules as for SFG but as a first approach should be feasible. Selection rules for SFG IR+Raman active, also the medium must not be version symmetric. **put the selection rules into the experimental details section?**

Tests with Born-effective charges: Intensities are also calculated via Born effective charges (BEC) where surface charges are determined and from that the intensities are obtained (dipole = charge*distance, $\mu^2 \propto I$).

Calculation of power spectra via velocity-velocity autocorrelation function from canonical MD trajectories. The vibrational density of states (VDOS) can be interpreted as the peaks of the spectrum. Through the motion of the atoms already some kind of quantum effects (not explicitly) are included.

$$VDOS(\omega) = \sum_{i=1}^N \int_{-\infty}^{+\infty} \langle v_i(t) \cdot v_i(0) \rangle e^{i\omega t} dt \quad (1.12)$$

1.6 Finding Transition States

One of the most prominent theories describing the transition state and the rate constants is Eyring theory of transition states **figure of reaction path?**. The most important approximations that are made are the following: all particles that reached the transition state will react towards the product. at the transition state geometry, the motion along the reaction coordinate can be separated from all other degrees of freedom and can be seen as a translation. The equation

1.7 From Density Functionals to Hybrids and Perturbation Theory

for the rate constant is described by

$$k(T) = \kappa \frac{k_B T}{h} e^{\Delta G^\ddagger(T)/(k_B T)}, \quad (1.13)$$

with the reaction rate constant k , Boltzmann's constant K_B , the temperature T , the difference of Gibb's free energy for the transition state and the educt ΔG^\ddagger and the transmission coefficient κ , that is a tunneling constant prefactor [tunneling corrections (seldomly applied in this work, not mention them here?)], give the reaction rate constant as a function of temperature and barrier height. For the latter one needs to find the energies of the transition state and the educt. The educt geometry can simply be obtained by geometry optimization as a minimum on the PES. To find the transition state geometry and henceforth the energy we used Nudged Elastic Band calculations (NEB), with Climbing Image, Reaction path is approximated as a series of associated images, which are connected via spring forces. These spring forces prevent the images from optimizing into the local minimum next to the transition state. First a regular NEB, then afterwards climbing image was done which gives better convergence. In this calculation the energetically highest image is "optimized" towards higher energies in the contrary direction of the gradient. For the point found by this scheme we checked whether this is a transition state via frequency analysis, since a TST of first order has to have one imaginary mode, that vibrates alongside the reaction path.

1.7 From Density Functionals to Hybrids and Perturbation Theory

In this work we also want to go beyond GGA (here the PBE functional), because it is known to underestimate reaction rates. Since we are interested in reaction kinetics it therefore is desirable to use more sophisticated methods to improve the rates. The first approach applied here is using hybrid functionals, where a fraction of exact exchange is mixed into the potential. Another ansatz is using Local Møller Plesset Perturbation Theory of 2nd order (LMP2) as implemented in crystal/crysccor. These calculations are way more computationally demanding but offer better results on a higher level of theory.

1.8 Computational Details and Used Programs

Vasp4.x, 5.2 and version x (newer), crystal, cryscor, cp2k+i-pi, Turbomole
For all the vasp calculations for the (0001) surface the parameters from prior work in our workgroup was used, like vacuum gap and convergence criteria, because these were converged carefully by Dr. Jonas Wirth. Convergence was achieved when energies between 2 SCF steps

1 Theory und Methodology

was smaller than 10^{-5} eV.

For (11 $\bar{2}$ 0) surface parameters were adopted and used as well. Also here the convergence criterion for the energy of 2 SCF cycles was 10^{-5} eV.

For the other programs that were not used before for the calculation of alumina in our group the geometries from the vasp output were used as starting points and the usual convergence criteria of the programs were applied with some exception when convergence was hard to achieve.

1.9 Experimental Techniques

In this work several experimental techniques were used from our collaborating group at the FHI, that is why the basics of those methods are explained shortly.

1.9.1 Vibrational Sum Frequency Generation

energy scheme, uv and IR/visible Laser beam are overlapped spatially and in time, polarization is important, s and p polarized, selection rules: IR and Raman active, specificity for surface only in systems that are not inversion symmetric, good for studying surface systems, no bulk signals (both solid phase and gas phase) due to selection rules

1.9.2 Thermal Desorption Spectroscopy

Sample is heated with a defined temperature program, adsorbates are removed from surface according their binding energies and detected as a function of temperature. Sheds light on adsorption strength and probable reaction networks.

1.9.3 Molecular Beam Source vs. Pinhole Dosing

When doing the experiment the method of preparation seems crucial for the results, because these result in different surface situations. Our collaborators use the so called Molecular Beam Source but many other experimental groups use pinhole dosing. Here the idea behind these methods and the main differences shall be explained.

pinhole dosing: water is brought with a high partial pressure onto the surface. Problem here: in the gas phase and on the walls of the measuring chamber can be amounts of water that can influence the measurement. this leads to an equilibrium situation.

MBS: A medium, e.g. water is probed onto the surface at a very low pressure. Non-equilibrium situations are generated by the kinetic energy of the beam.

1.9.4 Low-Energy Electron Diffraction

Spectroscopical method for determining crystal structures in crystalline materials by an electron beam with an energy in the range from 20 to 200 eV. Diffracted electrons are observed as a pattern on the fluorescent screen. Structure can be derived from the geometry of this pattern. Lattice geometry can be seen. Problem is the high energy of the beam that can lead to damage in the sample.

Other methods as tunneling based methods do not work on isolating materials like alumina, so that it is simply not possible to measure STM. Others? Rasterkraft? ATM?

2 Water on $\alpha\text{-Al}_2\text{O}_3(11\bar{2}0)$

2.1 Surface Model

The structure of α -alumina is well known for several years and was studied in many publications [cite here some](#). It crystallizes in the hexagonal cell, that means $\underline{a} = \underline{b} \neq \underline{c}$, with an angle of 60° between \underline{a} and \underline{b} .

To obtain the clean surface slab model a 2×2 supercell was cut from the bulk. The corresponding cell vectors were adopted from the bulk structure and a vacuum gap in z-direction (perpendicular to the surface) was introduced to avoid unphysical interaction between the slabs in z-direction. Since the $(11\bar{2}0)$ surface is not the crystal cut of the top of the shown crystal in figure 2.1(a), the cell vectors \underline{a} and \underline{b} are not equal as in the hexagonal cell, but $\underline{a} = 10.36\text{\AA}$, $\underline{b} = 14.16\text{\AA}$ and $\underline{c} = 20.5\text{\AA}$, with the angle between \underline{a} and \underline{b} of $\theta = 84.56^\circ$.

The unit cell consists of 5 atomic layers in z direction ($\text{O}-\text{O}_2-\text{Al}_4-\text{O}_2-\text{O}$), see Fig. 2.1(c)). The spacing between these layers in the relaxed structure and in the bulk crystal are given in Table 2.1. The supercell that is mostly used in this work has 10 layers, where the lowest 5 were fixed to the bulk value to mimic the surface situation. For the phonon calculations more layers were considered (up to 25 layers), see figure 2.2, here also for each slab size the lowest 5 layers were kept fixed, respectively (see chapter 2.4.1). The spacing between the 5 top layers is displayed in Table 2.1:

Table 2.1: Distances between the top 5 layers for different slab sizes and the unrelaxed bulk structure. All values are given in \AA .

| distance | atomic layer | | | | bulk |
|----------|--------------|-------|-------|-------|-------|
| | 10 | 15 | 20 | 25 | |
| d_{12} | 0.232 | 0.234 | 0.247 | 0.245 | 0.193 |
| d_{23} | 0.642 | 0.649 | 0.638 | 0.639 | 0.741 |
| d_{34} | 0.656 | 0.655 | 0.671 | 0.672 | 0.741 |
| d_{45} | 0.198 | 0.205 | 0.209 | 0.213 | 0.191 |

\mathbf{k} -point tests were done for 5 different grid sizes from $1 \times 1 \times 1$ to $5 \times 5 \times 1$. In contrast to the even grid sizes, the odd ones contain the Γ -point and therefore are favorable. It was shown that the $3 \times 3 \times 1$ grid is already converged with respect to the energy of the clean surface, see

2 Water on $\alpha\text{-Al}_2\text{O}_3(11\bar{2}0)$

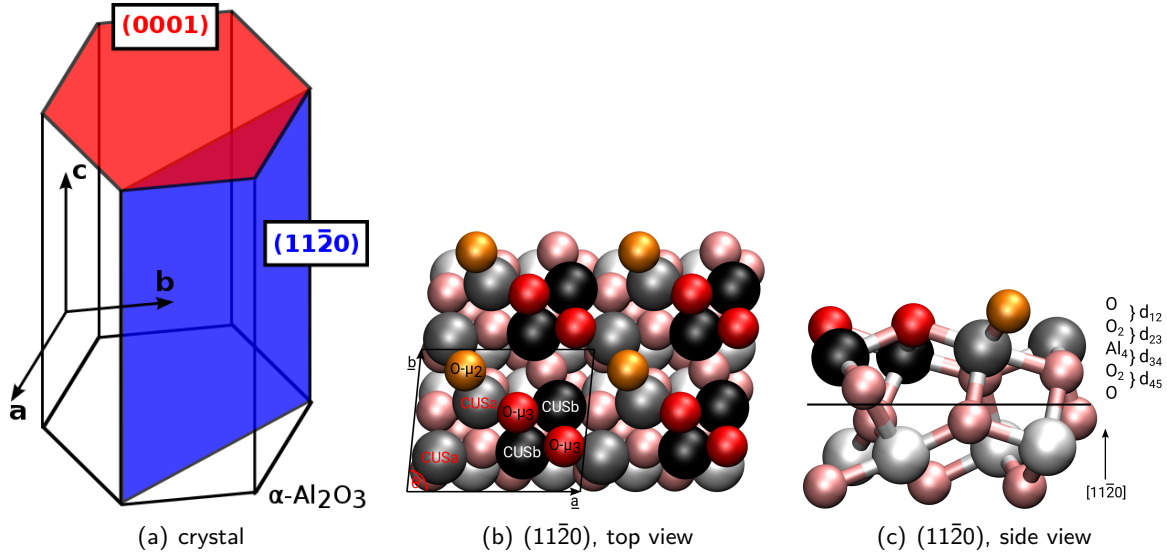


Figure 2.1: The crystal cut of $\alpha\text{-Al}_2\text{O}_3$, (a) schematic compared to the (0001) surface, (b) a top view of the geometry optimized unit cell with the nomenclature of the surface atoms and (c) as a side view showing the different atomic layers, see main text.

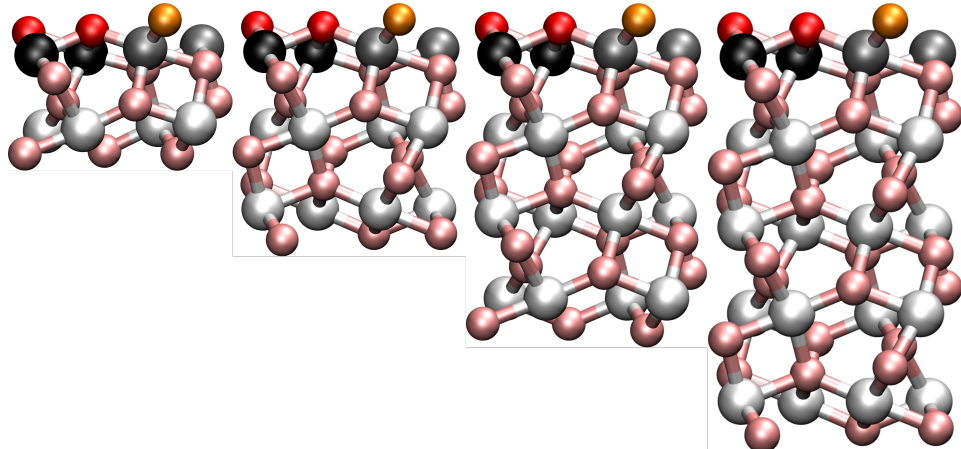


Figure 2.2: Side view for the different cell sizes from left to right 10, 15, 20 and 25 layers. Surface atoms are shown in the color code as used before.

Fig. 2.3.

Starting from this supercell approach there are 16 CUS Al-atoms (cordinatively unsaturated sites), these have less bonds than the aluminum atoms in the bulk structure since the surface layers has to be depleted. These atoms are very interesting for adsorbate molecules/atoms, because these atoms are electron rich and can be addressed for adsorption. If these 16 atoms are covered with adsorbates, here water, we get the system with 1 mono layer (ML). But one

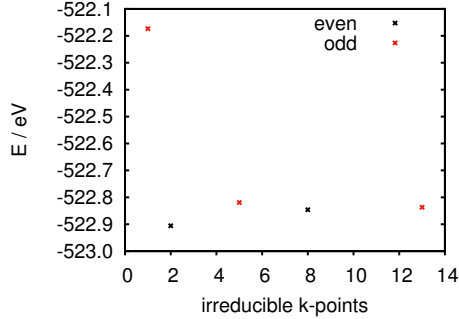


Figure 2.3: Sampling of the \mathbf{k} -points, shown is the energy of the super cell with respect to the number of irreducible \mathbf{k} -points. The even values correspond to the $2 \times 2 \times 1$ (2 irreducibles) and $4 \times 4 \times 1$ (8 irr.), whereas the odd, that contain the Γ -point, are described by $1 \times 1 \times 1$ (1 irr.), $3 \times 3 \times 1$ (5 irr.) and $5 \times 5 \times 1$ (13 irr.).

has to keep in mind the difference between these 16 surface atoms and the number of potential adsorbates: one monolayer is not built by 16 adsorbates since not all 16 CUS positions can be covered, but only 12, as is shown later (bridging water adsorption).

As is shown with different colors in figure 2.1 (b) and (c), the system consists of different types of CUS Al atoms with different coordination neighborhood and 2 different types of oxygen atoms, 2-fold and 3-fold coordinated. The Alumina atoms have the same number of oxygen neighbor atoms but differ slightly in the arrangement of their neighbors and the distance in the relaxed structure, but the oxygen atoms in fact differ by the number of neighbors. In this work, the black spheres denote the CUSb atoms, the grey ones depict the CUSA, the twofold coordinated oxygen atoms ($O-\mu_2$) are shown in yellow and the threefold coordinated ($O-\mu_3$) in red. Atoms of the underlying layers are illustrated in pale colors, light grey for alumina and pale red for oxygen.

2.2 Structure Search

acid base character of the adsorption, undercoordination of the alumina sites, bidentate adsorption, different types of Al and O cause large variety of possible adsorption sites First a low coverage regime was investigated: 1 water molecule per 2×2 supercell, which equals a coverage of 1/12. It was put on different positions on the surface and let relax. We found 1 molecular minimum and several dissociated species including both CUS and oxygen types, for adsorption energy and Gibb's free energy results see Table 2.2. There is also one metastable molecular species that seems more stable than the found molecular minimum, but since there is one imaginary mode displaying the movement of the proton towards the dissociated species

2 Water on $\alpha\text{-Al}_2\text{O}_3(11\bar{2}0)$

this cannot be classified as a stable minimum. The adsorption energy is defined by equation 2.1 as the energy of the adsorbed system compared to the energies of the clean surface and the isolated water molecule:

$$E_{\text{ads}} = E_{\text{ads. species}} - (E_{\text{free water molecule}} + E_{\text{surface}}). \quad (2.1)$$

The nomenclature for the adsorption sites that is used in the following gives at first the type of Al site where the OH-residue (OH^-) is adsorbed and at second place the oxygen type where the H(/H⁺) is adsorbed (OH-site||H-site). The notation with the / that will occur later denotes greater distances between the residues. The molecular minimum is substantially less stable

Table 2.2: change text! Adsorption energies as calculated from equation 2.1 for molecular and (singly) dissociated water on $\alpha\text{-Al}_2\text{O}_3(11\bar{2}0)$ according to periodic PBE+D2 calculations. Also the corresponding adsorption free energies G_{ads} at 130, 300 and 400 K defined analogously are also given. The three most stable configurations are in bold. All energies are given in eV.

| Adsorbed Species | | E_{ads} | $G_{\text{ads}, 130 \text{ K}}$ | $G_{\text{ads}, 300 \text{ K}}$ | $G_{\text{ads}, 400 \text{ K}}$ |
|------------------|-----------------------------------|------------------|---------------------------------|---------------------------------|---------------------------------|
| molecular | CUSb | -1.78 | -1.60 | -1.51 | -1.46 |
| dissociated | inter-CUSa O- μ_2 | -2.50 | -2.27 | -2.16 | -2.09 |
| | inter-CUSa O- μ_3 | -1.67 | -1.44 | -1.33 | -1.27 |
| | CUSb O-μ_2 | -2.28 | -2.12 | -2.03 | -1.97 |
| | CUSb O- μ_3 | -1.19 | -1.05 | -0.98 | -0.95 |
| | inter-CUSb O- μ_2 | -2.09 | -1.88 | -1.80 | -1.76 |
| | inter-CUSb O- μ_3 | -1.89 | -1.71 | -1.63 | -1.58 |

than the dissociated species. On the contrary, the dissociated water is very stable, also in comparison with the more stable surface cuts (0001) and (1 $\bar{1}02$) that were investigated before in our group by Dr. Jonas Wirth [?, ?]. Dissociated species, where the proton is located at a twofold coordinated surface oxygen is far more stable than the corresponding systems where the threefold coordinated is occupied, since the higher negative charge and the higher basicity of such a twofolded oxygen atom in comparison with the more saturated threefold coordinated O- μ_3 oxygen atom. Also the adsorption of OH at an inter-CUSa site is more favorable than at a CUSb site, because the former corresponds to a site where in the bulk system another oxygen atom would be situated, which is not the case for the CUSb position.

Dissociated species in direct neighborhood as shown in Table 2.2 and figure 2.4 are more stable than those where the proton and the OH residue are further apart (see Table 2.3), because the OH residue has a stabilizing effect on the H. In the table one can see, that the inter-CUSb||O- μ_3'' -species is more stable than the species inter-CUSb||O- μ_3' . This is due to the fact, that the periodic conditions lead to the decrease of the distance between OH groups again, so



Figure 2.4: change text! Adsorption geometries for molecular (a) and (six) dissociated water molecules ((b)-(g)) are shown, as obtained by periodic PBE+D2. The most favorable molecularly and dissociatively adsorbed configurations are shown. This means that we show nearest neighbor structures only (see text). The color code is the same as in Figure 2.1(b) and (c), CUSa grey, CUSb black, O- μ_2 yellow and O- μ_3 red; Hydrogen is displayed in white, subsurface layers are in pale colors.

that between 3 neighboring OH groups in the O- μ'_3 system the distances are 0.68 and 0.77 nm, whereas in the O- μ''_3 system the distances are 0.93 and 0.62 nm, where the latter one is closer by, so there is more stabilization. For examples of further diffusion reactions, see chapter 2.3.

Table 2.3: Comparison of next neighbor dissociated species and species where OH and H are further apart.

| Adsorbed Species | $E_{\text{ads}}[\text{eV}]$ |
|--------------------------|-----------------------------|
| inter-CUSA O- μ_3 | -1.67 |
| inter-CUSA O- μ'_3 | -1.42 |
| inter-CUSb O- μ_3 | -1.89 |
| inter-CUSb O- μ'_3 | -1.16 |
| inter-CUSb O- μ''_3 | -1.22 |

Systems with more layers were also studied and the adsorption energy results are shown in Table 2.4. Basically the results don't change much with increasing slab size. The molecular species is still less stable than most of the dissociated species, inter-CUSA||O- μ_2 is the most stable structure through all the sampled systems, inter-CUSb||O- μ_2 and CUSb||O- μ_2 change

2 Water on $\alpha\text{-Al}_2\text{O}_3(11\bar{2}0)$

their stability depending on the number of layers but still are some orders of magnitude less probable than inter-CUSa||O- μ_2 . Dissociated systems occupying the threefold coordinated surface oxygen atom are in the same stability order, relatively to each other. For higher number of layers, the inter-CUSb gets more favourable than CUSb, both for O- μ_2 and O- μ_3 . This might be due to less interaction between neighboring oxygen atoms with the inter-CUSb adsorbed OH group. This brings the point into attention that the system is already converged

Table 2.4: Adsorption energies calculated from equation 2.1 for molecular and dissociated species for different vertical slab sizes. All values are in eV.

| System | 10 layers | 15 layers | 20 layers | 25 layers |
|---|--------------|-----------|-----------|-----------|
| CUSb | -1.78 | -1.80 | -1.81 | -1.83 |
| inter-CUSa O-μ_2 | -2.50 | -2.46 | -2.54 | -2.56 |
| inter-CUSa O- μ_3 | -1.67 | -1.67 | -1.78 | -1.80 |
| CUSb O-μ_2 | -2.28 | -2.35 | -2.36 | -2.35 |
| CUSb O- μ_3 | -1.19 | -1.71 | - | - |
| inter-CUSb O-μ_2 | -2.09 | -2.43 | -2.48 | -2.36 |
| inter-CUSb O- μ_3 | -1.89 | -1.59 | -1.65 | -2.09 |

for the 10-layer slab referring to adsorption energies (and also vibrational OH/OD frequencies as can be seen later in section 2.4.1).

Also systems with a higher water coverage were considered, some cases for 2 water molecules, 4 inter-CUSa||O- μ_2 and a fully covered supercell, for these systems also normal mode analyses were done to get vibrational spectra, see also chapter 2.4.1.

The stability of those species with higher water coverage is defined as

$$E_{\text{ads}} = E_{\text{ads. species}} - (E_{\text{free water molecule}} \times n + E_{\text{surface}}), \quad (2.2)$$

with n being the number of water molecules adsorbed on the surface. In Table 2.5, the adsorption energies are given. Comparing these results for the higher coverages to results with only one adsorbate, just by adding the adsorption energy one can see the following (see also column 3 in Table 2.5): For all systems the added energy of the singly adsorbed species is more stable than the doubly adsorbed water systems. Instead of stabilizing the whole system, they are destabilized by the adsorption neighborhood, even in structures that contain hydrogen bonds.
do neighbors stabilize molecular adsorption?? In Phonon paper, Eads(Cb+Cb2)=-4.57eV, sum of the two individually is -4.06eV, so there is in fact a stabilizing effect!, For inter-CUSa||O- μ_2 +CUSb||O- μ_2 there is no effect and for inter-CUSa||O- μ_2 inter-CUSa||O- μ_2 , there is clear destabilization!

What is the respective coverage? 0.xyML

2.3 Reactions and Microkinetic Model

Table 2.5: Adsorption energies in eV for higher water coverages. For comparison in the third column the added energies for singly adsorbed water are shown.

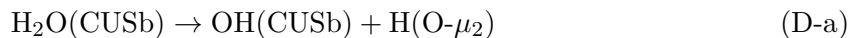
| Adsorbed Species | E_{ads} | isolated species |
|--|------------------|------------------|
| CUSb(mol)+CUSb O- μ_2 | -4.57 | -4.06 |
| inter-CUSA O- μ_2 +CUSb O- μ_2 | -4.77 | -4.78 |
| 2inter-CUSA O- μ_2 | -4.84 | -5.0 |
| 4inter-CUSA O- μ_2 | -9.55 | -10.0 |
| 12H ₂ O | -23.39 | <i>a</i> |

a One can not distinguish exactly, but there are 4 inter-CUSA-OD groups, 8 CUSb-OD groups, 8 O- μ_3 and 4 O- μ_2 OD groups, hence one can not calculate a sum of the isolated species.

2.3 Reactions and Microkinetic Model

Based on the minimum structures one has to identify reaction pathways to fully understand the reactivity of a system, so we utilize the NEB method including Climbing Image to search for transition states between the minima. We examined 3 different types of reactions: dissociation from the molecular minimum, as well as OH- and H-diffusion. The dissociation reactions are named D, diffusion reaction with Df-OH and Df-H, respectively, in Table 2.6 and figures 2.5 and 2.6. In reference [11-20paper](#) only some reactions were introduced, additional reactions paths are given here.

We investigated 5 different dissociation reactions. The two that were already shown in the publication [11-20paper](#) are the reactions from CUSb to the twofold coordinated oxygen (D-a) and one to the threefold coordinated O (D-b). One additional dissociation starts from the metastable inter-CUSA molecular structure that is, as was shown before, no minimum structure and goes to the most stable species inter-CUSA||O- μ_2 (D-c). 2 further dissociation reactions converged but showed a two step process and are therefore not interesting in the first place (these reactions are CUSb→inter-CUSA||O- μ_2 and CUSb→inter-CUSb||O- μ_2 and both went via the dissociated CUSb||O- μ_2 intermediate [put them into appendix?](#)). As can be seen from chapter 2.2 (Table 2.2), the molecular minimum CUSb is very low in stability compared to the dissociated minima. The reaction D-a leads from the molecular minimum at CUSb to the twofold coordinated CUSb||O- μ_2 :

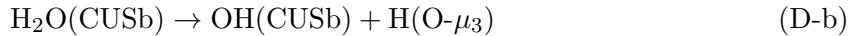


The barrier is very low, about 0.002 eV as one can see from Table 2.6 and figure 2.5(a), hence the reaction rate constant is very high, in the range of $k_{300\text{K}} = 10^{12} \text{ s}^{-1}$. This low barrier might be due to underestimation of barrier heights with the used functional PBE (compare chapter

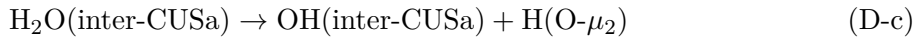
2 Water on $\alpha\text{-Al}_2\text{O}_3(11\bar{2}0)$

citation x, 1.7).

For the other dissociation reaction D-b from CUSb to CUSb||O- μ_3 , there is no barrier found at all, the reaction pathway shows simply an upgoing path in energy without any barrier, since the molecular minimum is by 0.15 eV more stable than the dissociated structure on CUSb||O- μ_3 . Thus, no reaction rate constant can be calculated.



A further dissociation D-c from the metastable inter-CUSA species also shows no barrier, probably because the educt is no stable minimum and because the product is much more stable:



On the other hand reaction D-b does also not show a barrier, so it remains unclear whether it is due to methodology or the barrier is too low to be detected with the settings applied for the calculations.

Apart from dissociation that is highly favoured on this surface cut compared to more stable alumina surfaces, diffusion reactions starting from the dissociated species are important for understanding processes. The OD diffusion reaction Df-OH-a moves from CUSb||O- μ_2 to the inter-CUSb position, which is relatively fast for OD diffusion reactions compared to the reactions at other alumina surfaces [cite Jonas](#).



In this special reaction, the OH residue diffuses from an on top CUS position into a gap between two CUSb atoms, so that there is not much repulsion with neighboring surface oxygen atoms and other CUS atoms nearby during the diffusion. Also the distance that has to be bridged is very small. The barrier height equals 0.35 eV and the corresponding rate constant $k_{300\text{K}} = 1.88 \times 10^6 \text{s}^{-1}$. In contrast to that the real CUS-to-CUS reaction Df-OH-b that is much slower. It is a diffusion from CUSb to inter-CUSA with the hydrogen residue staying at an O- μ_2 position. This barrier is with 1.07 eV relatively high and leads to $k_{300\text{K}} = 2.41 \times 10^{-6} \text{s}^{-1}$.



This is still faster than OH diffusion reaction for the (0001) alumina surface ([cite Jonas](#) and compare to doctoral thesis of Dr. Jonas Wirth, UP 2016), where the rates constant $k_{300\text{K}} = 4 \times 10^{-45} \text{s}^{-1}$. For the (1102) surface there was no OH diffusion calculated, but the corresponding

2.3 Reactions and Microkinetic Model

H_2O diffusion process is around $k_{300\text{K}} = 1.4 \times 10^{-3}\text{s}^{-1}$, whereas the H_2O diffusion process for the (0001) surface is in the range of $k_{300\text{K}} = 8 \times 10^{-3}\text{s}^{-1}$, too. For the (11 $\bar{2}$ 0) surface no H_2O diffusion reactions can be observed due to the instability of the molecularly adsorbed species that would rather dissociate than diffuse.

A larger variety can be achieved when looking at H diffusion reactions. The different types of surface oxygen atoms and also the distances between OH and H residue make differences in the observed reactions. As seen before, the hydrogen is preferably found on the twofold coordinated oxygen atom, but the reaction to a neighboring threefold coordinated oxygen is possible and opens the gate to structures with greater proximity. The reaction takes place with the OH residue being on a CUSb site:



The reaction shows a barrier height of 0.95 eV, but the NEB transition state has no imaginary frequency so that no rate can be derived, although the NEB path clearly shows a smooth barrier profile. An analogue reaction starting from the most stable inter-CUSA||O- μ_2 to the threefold coordinated oxygen is reaction Df-H-b:



the barrier of the free energy is 1.50 eV, rate constant at 300 K of $4.90 \times 10^{-13}\text{s}^{-1}$. This process is so unlikely because a less favored O- μ_3 position is occupied and this position is also less stabilized by reason of the greater distance of OH_{surf} and OH_{ads} groups. This reaction increases the distance to a position further away than next neighbor. As mentioned before, the nomenclature for these structures uses different amounts of primes (\prime) to display the distance. A similar reaction for the OH sitting on inter-CUSb and the hydrogen being adsorbed on an O- μ'_2 position, diffusing further away to O- μ''_3 , which is less in stability:



The free energy barrier is relatively high with 1.30 eV leading to a rate constant $k_{300\text{K}} = 9.96 \times 10^{-1}\text{s}^{-1}$. The ' in the equation above is set in parentheses because it is the nearest possible O- μ_2 position, but not the nearest possible distance from the OH_{ads}.

Going one step further from reaction Df-H-d, the last reaction leads to the position where OH and H have the greatest possible distance with the applied periodic bounding conditions:



2 Water on $\alpha\text{-Al}_2\text{O}_3(11\bar{2}0)$

With an energy barrier of 0.94 eV the rate at 300 K is $1.1 \times 10^{-3}\text{s}^{-1}$.

Possible path from inter-CUSb||O- μ_3' to O- μ_3' to O- μ_3'' and to the furthest possible O- μ_3''' . The first reaction was calculated but did not converge for unknown reasons. The two next steps of this hydrogen migration path were studied..

Table 2.6: CHANGE THIS TABLE COMPLETELY!! Reaction rates for selected reaction paths examined. $\Delta E = E(\text{product}) - E(\text{educt})$, $\Delta E^\ddagger = E^\ddagger - E(\text{educt})$, respectively for the free energy, G , obtained from PBE+D2 calculations. k is the rate constant from eq. (1.13). Thermodynamic quantities and rates are given for $T = 300$ K. "n.f." indicates "not found". The reactions are either water dissociation (D), OH diffusion (Df-OH) or H diffusion (Df-H).

| Reaction Type | ΔE (eV) | $\Delta G_{300\text{ K}}$ (eV) | ΔE^\ddagger (eV) | $\Delta G_{300\text{ K}}^\ddagger$ (eV) | $k_{300\text{ K}}$ (s^{-1}) |
|-----------------------------------|-----------------|--------------------------------|--------------------------|---|--|
| H_2O dissociation | D-a | -0.50 | -0.52 | 0.01 | 5.76×10^{12} |
| | D-b | 0.59 | 0.53 | n.f. | n.f. |
| | D-c | | | n.f. | n.f. |
| OH diffusion | Df-OH-a | 0.19 | 0.22 | 0.35 | 1.88×10^6 |
| | Df-OH-b | -0.21 | -0.13 | 1.07 | 2.41×10^{-6} |
| H diffusion | Df-H-a | | | no TST | |
| | Df-H-b | 1.08 | 1.04 | 1.65 | 4.90×10^{-13} |
| | Df-H-c | 0.93 | 0.89 | 1.36 | 9.96×10^{-10} |
| | Df-H-d | -0.06 | -0.07 | 1.05 | 1.05×10^{-3} |

As mentioned before a huge well known problem of GGA is that barriers are underestimated. Optimizing structure with HSE06 is nearly impossible due to high cost and doing single point calculations on PBE optimized transition state is not very accurate and doesn't deliver better results (see also work of Dr. J. Wirth). (at least for crystal calculations... so don't bring it her?)

Proton diffusion reactions are way more variable giving reaction rates at 300 K ranging from 10^{-13} to 10^{-3}s^{-1} . The barriers and therefore also rate constants for H-diffusion cover a wider range depending on the distance between OH and H and of course more importantly on the fact between which type of O $\mu_{2/3}$ the proton is diffusing.

Also reactions leading to a not next-neighbored situation, increasing the distance between OH and H are also not favorable since geometries with the residues further apart are energetically less stable.

Rates for backreactions can also be calculated and the results are shown in Table 2.7.

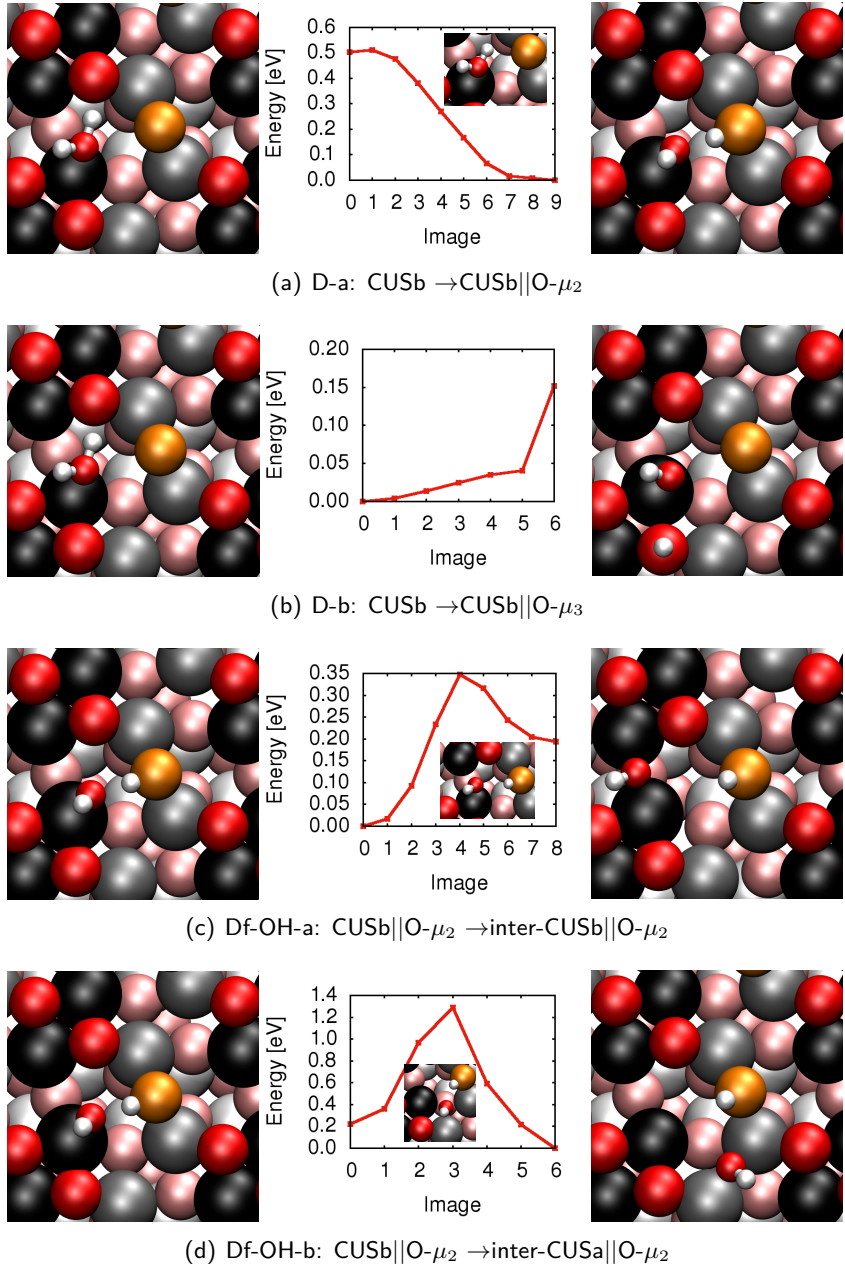


Figure 2.5: Minimum energy paths with transition states (inlay; if available), and both educt (left) and product (right) states for D-a, D-b, D-c, Df-OH-a and Df-OH-b reactions, respectively. The color code is as explained above.

2 Water on $\alpha\text{-Al}_2\text{O}_3(11\bar{2}0)$

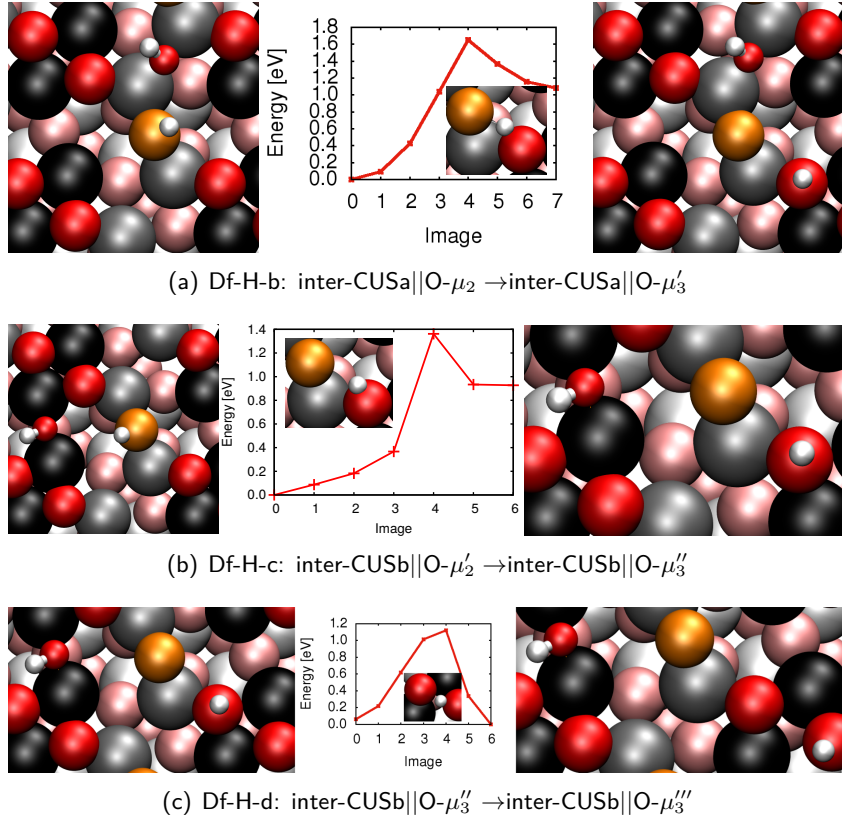


Figure 2.6: Minimum energy paths with transition states, and both educt and product states for Df-H-b - Df-H-d reactions. The color code is as explained above.

Table 2.7: Reaction rate constants for the backreactions in comparison with forward reactions (left). These rates can be calculated via detailed balance $\frac{\leftarrow}{\rightarrow} k = k e^{-\Delta G/k_B T}$. All values are given in s^{-1} and at a temperature of 300 K.

| Reaction Type | $k_{300 \text{ K}}(\text{s}^{-1})$ forward reaction | $k_{300 \text{ K}}(\text{s}^{-1})$ back reaction |
|---------------|--|---|
| D-a | 5.76×10^{12} | 1.17×10^4 |
| D-b | n.f. | n.f. |
| D-c | n.f. | n.f. |
| Df-OH-a | 1.88×10^6 | 9.86×10^9 |
| Df-OH-b | 2.41×10^{-6} | 1.69×10^{-8} |
| Df-H-a | <i>no TST</i> | <i>no TST</i> |
| Df-H-b | 4.90×10^{-13} | 1.49×10^5 |
| Df-H-c | 9.96×10^{-10} | 9.95×10^5 |
| Df-H-d | 1.05×10^{-3} | 7.12×10^{-5} |

2.4 Vibrational Frequencies / Spectroscopic Properties

A great source of knowledge about chemical systems is vibrational spectroscopy, so we were interested in frequencies of the systems, since the frequencies of these vibrations give us hints about the chemical environment as hydrogen bonds and other atoms nearby that bond to each other. These vibrational frequencies were calculated for the surface system adsorbed with OH and also with OD. Our experimental partners from FHI use deuterated water (D_2O) instead of H_2O because the chemical reactivity is the same but the spectroscopic properties are better with their applied Laser system. The experimental SFG spectra (Sum Frequency Generation) for the OD range of the low coverage regime for two different coverages are shown in Fig. 2.7. Of course, the frequencies for a deuterated system are different from OH, but the different

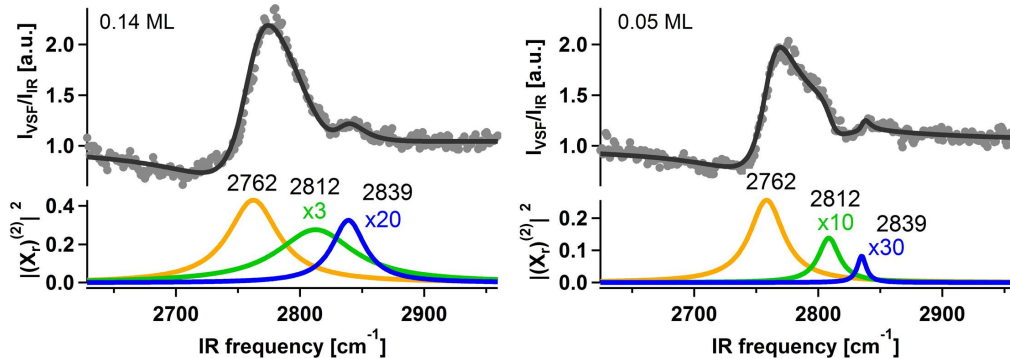


Figure 2.7: Experimental SFG results for $(11\bar{2}0)$ surface with 0.14ML (mono layer, left spectrum) and 0.05ML water coverage (right) including fit. The experiment was conducted by Yanhua Yue, FHI Berlin. Coverage only influences intensity of the peaks but not the peak position itself. The different coverages are achieved via different preparing temperatures of the sample.

isotopes can be calculated easily within vasp, just by changing the mass.

Better put this in theory part? In experiment the alumina single crystal was cleaned in ethanol and Milli-Q water and dried with N_2 before being installed in the ultra high vacuum chamber. It was then sputtered in Ar, and annealed to high temperatures in UHV and afterwards three times in oxygen at different temperatures. After this treatment, D_2O was brought onto the surface with a molecular beam source. For further details see cite11-20paper and the supporting information.

To calculate the modes in this work mainly two methods were applied: Normal mode analyses (see section 2.4.1) and for some systems also power spectra from *ab-initio* MD via velocity-velocity autocorrelation function (section 2.4.2).

We focus mainly on the position of the peaks rather than the intensities, because in the first place it is of greater interest what kind of vibrations gives which peak than the intensity of

2 Water on $\alpha\text{-Al}_2\text{O}_3(11\bar{2}0)$

this peak. It is also still challenging to get the frequencies right before heading to intensities. In the power spectra from MD calculations the intensities are implicitly received and for the normal mode analyses this work follows 2 different approaches, dipole corrections and Born effective charges.

In subsection 2.4.1, also modes for higher coverage systems are also examined.

But not only the OH/OD frequencies are of interest, but also the lattice vibrations, and are covered in both subsections.

2.4.1 Normal Mode Analysis

OD Vibrations

The normal modes are within the harmonic approximation and depend on the mass and the spring constant of the bond. This ansatz is quite good for high frequency modes like OD stretch vibrations. We assumed that the OD stretching modes for the 3 most stable structures would contribute to the spectrum the most (see Table 2.8). Of course, all molecular and next

Table 2.8: Comparison of the different slab sizes (normal modes): OD stretching modes for each of the most stable minima. In parantheses, the angle of the OD bonding vector to the surface normal (θ in $^\circ$) is given. The left value reflects the adsorbed OD group and the right wavenumber the surface OD group, respectively.

| Layers | inter-CUSa O- μ_2 | CUSb O- μ_2 | inter-CUSb O- μ_2 |
|--------|------------------------|----------------------|------------------------|
| 10 | 2731 (44), 2694 (36) | 2785 (26), 1711 (61) | 2692 (41), 2689 (54) |
| 15 | 2728 (44), 2695 (36) | 2783 (24), 1812 (60) | 2711 (34), 2656 (60) |
| 20 | 2729 (44), 2694 (35) | 2783 (24), 1838 (60) | 2715 (34), 2665 (58) |
| 25 | 2728 (44), 2696 (35) | 2767 (59), 1750 (62) | 2764 (29), 2724 (41) |
| exp. | | 2839, 2812, 2762 | |

neighbor dissociated structures from 10 to the 25 slab layer model were calculated, although as it was mentioned in section 2.2 that the slab was already converged with 10 layers concerning OD stretch frequencies. Following this approach we expect 6 modes, for each of the three an OD_{surf} and an OD_{ads} . In all cases the relationship between the two individual modes for each considered structure is portrayed by $\tilde{\nu}(\text{OD}_{ads}) > \tilde{\nu}(\text{OD}_{surf})$. This can be explained with the different reduced mass for both vibrations: The OD_{surf} oscillator has a slightly larger reduced mass since the deuterium is bound directly to the surface, whereas the adsorbed OD group can act more as a quasi-free OD group [citekirsch2014](#). All these vibrations are clearly localized on one of the OD groups, which suggests that the normal modes ansatz is reasonable.

To consider the probability of observing these species, we calculated their respective Boltzmann

2.4 Vibrational Frequencies / Spectroscopic Properties

weights P_i :

$$P_i = e^{-G_i/(k_B T)}. \quad (2.3)$$

With this analysis it is possible to show the relative population for different temperatures, see Table 2.9. In the whole temperature range relevant for the experiments, it is shown that the population of the species inter-CUSa||O- μ_2 clearly dominates and that the population of inter-CUSb||O- μ_2 is very low, compared to the others.

Table 2.9: Boltzmann population relative to the most stable inter-CUSa||O μ_2 , calculated according to eq. 2.3.

| | P _{130K} | P _{300K} | P _{400K} |
|------------------------|-----------------------|----------------------|----------------------|
| inter-CUSa O- μ_2 | 1 | 1 | 1 |
| CUSb O- μ_2 | 1.4×10 ⁻⁶ | 6.1×10 ⁻³ | 3.2×10 ⁻² |
| inter-CUSb O- μ_2 | 1.0×10 ⁻¹⁵ | 1.2×10 ⁻⁶ | 6.6×10 ⁻⁵ |

With the results for the frequencies of the three most stable structures (here the inter-CUSb||O- μ_2 results are shown for completeness), one can see, that for all slab sizes, there are 4 relevant modes. One of them is noticeable lower in energy that is due to hydrogen bonding. Also the angle of the bonding vector with respect to the surface normal is very high (i.e. the bond is more in plain, values shown Tab. 2.8, schematic representation in Tab. 2.10) so that the expected intensity in experiment is remarkably lower and may be not visible in experiment because of the angle dependence of the intensity in VSF.

With this in mind, we are able to predict 3 peaks, which fits well to the experimental results (see Fig. 2.7). Comparing these results in absolute numbers is not very convincing as before in the literature, but relative numbers are in good agreement (see results for experiment and all different sized layer slabs in Table 2.10).

Table 2.10: Frequency differences $\Delta\tilde{\nu}$ are given in [cm⁻¹]. $\Delta\tilde{\nu}_1$ depicts the difference between the surface OD group of the inter-CUSa||O- μ_2 species and the respective surface OD group on O- μ_2 and $\Delta\tilde{\nu}_2$ is the difference between the same surface OD group and the adsorbed OD group on CUSb from CUSb||O- μ_2 . In the right half a sketch of the angle θ between the OD bond and the surface normal is shown.

| layers | $\Delta\tilde{\nu}_1$ | $\Delta\tilde{\nu}_2$ | |
|--------|-----------------------|-----------------------|--|
| 10 | 37 | 91 | |
| 15 | 33 | 88 | |
| 20 | 35 | 89 | |
| 25 | 32 | 71 | |
| exp. | 50 | 77 | |

2 Water on $\alpha\text{-Al}_2\text{O}_3(11\bar{2}0)$

Two problems of this approach are, that we neglect anharmonicities, that are especially important for hydrogen bonded vibrations and also the absence of neighbor effects, that can be solved by computing higher coverage systems.

The influence of higher coverage was examined for some test systems already presented in section 2.2. The coverage differs from 2D₂O molecules per super cell to 4 and 12 water molecules (equals 1ML). **Here the frequencies of the OD stretching modes are affected due to the neighbor effects, for some structures more and for other less (e.g. the system with 2inter-CUSa||O- μ_2). compare modes of low coverage limit to spectra with higher coverage, ask Lu for more data of higher coverage.**

The simulation of intensities was done both with dipole corrections and Born effective charges and is shown here as a comparison. *show only high frequency part, comparing BEC and dipole, for the most stable configurations. These are only IR intensities in both cases, that can not be set equal to SFG intensities but can be a first hint.*

Frequencies for the low coverage limit were also calculated using the crystal code, that enables calculations with atomic centered bases and makes it possible to treat a real 2-D system without the need to calculate the repetition of the slab in z-direction, see also section 3.3.1. With this code it is also possible to calculate hybrid functionals, here B3LYP easily. For both PBE and B3LYP, geometries of the most stable states were optimized and from those geometries normal modes were calculated. Also anharmonicities for OH/OD bonds could be calculated, results in comparison with vasp results are shown in Table 2.11. First of all, PBE results from both programs do not differ largely. anharmonicities decrease the wavenumbers and lead to worse agreement to experiment and to vasp calculations. Data from B3LYP calculations show great agreement with experiment, although here, anharmonic corrections make the agreement worse, too. One has to mention, that here influence of the basis set is strong and larger basis sets were not feasible due to high computational costs.

Lattice Vibrations

For the phonons as a first test the same normal modes analyses were checked to get a first impression into how the spectra can look like. But for a better description we need to consider more layers of the bulk in order to get more reliable results. From an experimental point of view it is suggested that SFG spectra can give insight into x layers of the bulk **ask Lu!**. Therefore we did calculations for the most stable adsorption geometries for more layered systems, going up to 6*5=30 layers (with 5 being the number of layers in the unit cell in z direction), both for the clean surface and for the adsorbate covered surface, here we used again optimized geometries of the most stable structures. These results are also shown with intensities calculated from

Table 2.11: Stretch wavenumbers for both of the OD groups at the (11 $\bar{2}$ 0) surface for the 3 most stable species, calculated with atom centered basis functions with the program crystal. Frequencies were calculated at the B3LYP and PBE level of theory, optimized with the respective method. The used basis set was pob_TZVP. The VASP results were obtained with a plane wave basis and PBD+D2 corrections.

| stretch | PBE | | B3LYP | | VASP result $\tilde{\nu}$ [cm $^{-1}$] |
|--------------------------|-----------------------------|-------------------------------------|-----------------------------|-------------------------------------|--|
| | $\tilde{\nu}$ [cm $^{-1}$] | $\tilde{\nu}$ +anharm [cm $^{-1}$] | $\tilde{\nu}$ [cm $^{-1}$] | $\tilde{\nu}$ +anharm [cm $^{-1}$] | |
| iCa2: OD _{surf} | 2682 | 2599 | 2773 | 2695 | 2694 |
| iCa2: OD _{ads} | 2728 | 2644 | 2811 | 2729 | 2731 |
| Cb2: OD _{surf} | 1658 | 1310 | 2019 | 1722 | 1711 |
| Cb2: OD _{ads} | 2769 | 2687 | 2843 | 2765 | 2785 |
| iCb2: OD _{surf} | 2657 | 2595 | 2778 | 2694 | 2689 |
| iCb2: OD _{ads} | 2688 | 2569 | 2777 | 2689 | 2692 |

dipole corrected normal mode analyses. The additional geometries with more layers do not differ strongly from the 10 layer ones that were presented in section 2.2.

Table with no. of layers and adsorption energies? Put it to section 2.2? Probably better do do it there! compare clean surface for different sizes, iCa2, Cb2 and iCb2 for all slab sizes. Normal modes may not be a perfect description of these deeply delocalized vibrations.. intensities for lattice vibrations from BEC and dip..

2.4.2 Velocity-Velocity Autocorrelation Function

Extract vel vel autocorrelation function from MD at 300 K (and also 400 K?) from most stable structures (inter-CUSa||O- μ_2 , CUSb||O- μ_2 and inter-CUSb||O- μ_2), with Fourier transformation converted to VDOS spectrum. It also is possible to separate modes from water layers from bulk phonons. Not really important if you don't use hydroxylated surface with a higher water coverage? So for Giacomo's system it makes sense, but here it is unnecessary.

totally different ansatz, no freq analysis, no harmonic approximation, but ab-initio MD trajectories at 300K, starting from optimized minimum structures. trajectory duration of 1-a few ps. calculating vac, fourier transform gives power spectra, no real IR, but still one can relate to intensities. results for trajectories.

2.5 Desorption Process

Not only the reactions at the surface are of interest but also the process of adsorption and desorption were studied. The experimentalist's method to do so is TPD (thermal desorption spectroscopy). It is possible to measure the bond strength of the adsorbates, depending on

2 Water on $\alpha\text{-Al}_2\text{O}_3(11\bar{2}0)$

the temperature they can be found in the corresponding spectrum. The sample was flashed to 400 K to get rid of impurities. The results showed two peaks, one beneath 400 K and one above. This peak beneath 400 K should not be visible, since the sample was heated to that temperature and all adsorbates that are released beneath this temperature should not be there any more. The only plausible explanation to this is, that there are reactions, that fill this species up and so the desorption can still be from this species.

To interpret these results, one has to think of a possible reaction scheme from the most stable adsorption sites via the molecular state leading to the gas phase molecule.

Here the most stable inter-CUSA \parallel O- μ_2 , CUSb \parallel O- μ_2 and inter-CUSb \parallel O- μ_2 and their reactions
not sure if this is worth a whole chapter..

calculation with NEB was not done, instead geometry optimization for a water molecule above 3 interesting points on the potential energy surface (above inter-CUSA, CUSb and inter-CUSb).

`/und/sophia/bigger-cell_newcrystalcut/2x2cell/2layers/gasphase-physisorbed`

It was also tried to study the adsorption/desorption process (not with NEB), since there was no minimum structure in the gas phase nor physisorbed state. But from a single water molecule above the surface, geometry optimizations were done. Three structures were tested above inter-CUSA, CUSb and inter-CUSb. The energy profile is smooth from any tested point on the potential energy surface above the alumina surface towards the adsorbed water system without showing a barrier but indeed both showing an intermittent molecularly adsorbed structure.

As mentioned before the experimentalists measure TPD in order to understand the adsorption strength and possible exchange reactions. We tried to simulate the desorption process using the following scheme: take the water in the gas phase + the clean surface as the standard. In the thermal equilibrium, the water should be equally distributed to Boltzman's distribution in the most stable structures. From this situation the water can recombine to the molecularly adsorbed water. The recombined water then can desorb to the gas phase. Since the spectrum is measured in ultra high vacuum it can be assumed that all the water that has left the surface will not return to the system, because it is dragged out of the equilibrium by the vacuum pumps. Applying the reaction rates of the corresponding reactions in a kinetic Monte Carlo approach leads to **Redo these calculations? I don't think that this is worth the effort...**

does it make sense to bring this cause there is no good agreement between our theory and the experimental findings..? The NEB didn't lead to anything since there is no minimum (just try a NEB??), optimization doesn't show any kind of barrier and just modelling the desorption from the rates is not good enough, since the rate for Cb2-Cb is too small to

3 Water on $\alpha\text{-Al}_2\text{O}_3(0001)$

The (0001) surface is the most stable surface site of alumina under UHV conditions, and was subject of several studies so far. Both experimental and theoretical studies discovered lots of characteristics and specialties of this crystal cut. In our workgroup previous work was done concerning the stability of low limit water coverage and their vibrational spectroscopic behaviour, reaction pathways between these stable minima, but also studying higher water coverages and hydroxylated surface systems. In this work, the focus lies more on two topics:

- (i) understanding the processes of a water molecule (D_2O) being shot at the surface with a molecular beam source with the help of *ab-initio* Molecular Dynamics and
- (ii) the improvement of reaction rates with different methods beyond GGA functionals (as PBE).

First, the surface and the most stable adsorption patterns are introduced (section 3.1), followed by the results for the molecular beam scattering (section 3.2) and last the improvements for the reaction rates (see section 3.3).

3.1 Surface Model and Static Calculations

The most stable surface cut is a stoichiometric, Al terminated one, and in contrast to the $(11\bar{2}0)$ surface there is only one type of Al-CUS atom, which is a reactive Lewis-acid site. Also, all oxygen atoms are 3-fold coordinated, that leads to a topography that is not as complex as for the higher indexed surfaces. We applied here a 2×2 supercell with vectors that were optimized from the bulk structure vectors (previous work of J. Wirth). The surface slab consists of 9 atomic layers, that is three repeating units in z direction of the type Al-O₃-Al..., with the top 5 layers being allowed to relax during optimization and AIMD and the lowest 4 layers being fixed to bulk values, see Fig. 3.2. The unit cell vectors in there are equal to $a = b = 9.66 \text{ \AA}$ and a 60° angle between them. The c -vector of the slab model is 31.4 \AA long, hence the vacuum gap between two slabs in this direction is 26.4 \AA .

The stability, vibrations and reactivity of one water molecule per 2×2 supercell were already studied by Dr. Jonas Wirth. As it was published in refjonas0001, there is one molecular minimum on top of a CUS atom and 3 dissociated states (see figure 3.3): the next neighboring

3 Water on $\alpha\text{-Al}_2\text{O}_3(0001)$

1-2 dissociated state, the 1-4 dissociated structure with the Hydrogen atom being one position further and the 1-4' that is the configuration with the greatest distance that is possible for this slab size. From these, the 1-2 dissociated species is the most stable one and the 1-4' is the least stable one. For the stability of the molecular and the 1-4 dissociated species, the situation is more controversial in the literature. In our periodic DFT studies with VASP, it lies between the previously mentioned ones, depending on the exact method employed, for PBE+D2 the molecular adsorbed species is more stable than 1-4, for PW91+D2 the 1-4 dissociated is more stable, whereas PW91 without dispersion corrections gives the same adsorption energy for both species (the values for the adsorption energy are calculated analogously to the (11 $\bar{2}$ 0) surface cut, see eq. 2.1). Calculations with an atom centered basis instead of plane waves with the crystal code show, that for most basis sets the molecular species is more stable and for others, they are both equal in adsorption energy.

Of course, there are reactions linking these minima, dissociation, OH- and H-diffusion were studied, as well as rotation of an OH group and molecular water diffusion from CUS to CUS. The latter two do not play a crucial role in this work, especially the CUS to CUS diffusion of molecular water is very improbable due to the slow reaction rate. Adsorption energies and reaction rates that are important for this work are shown in Table 3.1, these results were obtained by J. Wirth and were unpublished.

Table 3.1: Adsorption energies for the stable minima (left part) and reaction rate constants k in s^{-1} at 300 K with corresponding barrier heights ΔG^\ddagger in eV for the processes connecting these minima (right part). Here the upper two line shows the reaction in the direction given in the name and the lower two line gives the back reaction's rates constants and barriers. All values were calculated with PBE including D2 dispersion corrections and are unpublished work of J. Wirth.

| mol | E _{ads} [eV] | | | k _{300K} [s^{-1}] | | | | |
|-------|-----------------------|-------|-------|---------------------------------------|----------------------|-------------------|-------------------|-------------------|
| | 1-2 | 1-4 | 1-4' | diss-1-2 | diss-1-4 | diff-2-4 | diff-2-4' | diff-4-4' |
| -1.31 | -1.69 | -1.30 | -1.21 | 8.0×10^{10} | 2.8×10^{10} | 2.7×10^1 | 3.8×10^1 | 7.1×10^5 |
| | | | | 0.13 | 0.19 | 0.82 | 0.81 | 0.61 |
| | | | | 2.3×10^4 | 2.7×10^{10} | 9.1×10^7 | 3.1×10^9 | 1.7×10^7 |
| | | | | 0.50 | 0.19 | 0.44 | 0.33 | 0.51 |

The adsorption process itself was studied, by starting from the molecular minimum, gradually doing optimizations with greater O-surface distance and letting everything relax except for the c-coordinate of the water-oxygen atom. This calculations gives an energy profile for the adsorption/desorption but no barrier could be found (see Fig. 3.1), so the underlying adsorption process is thought to be barrierless.

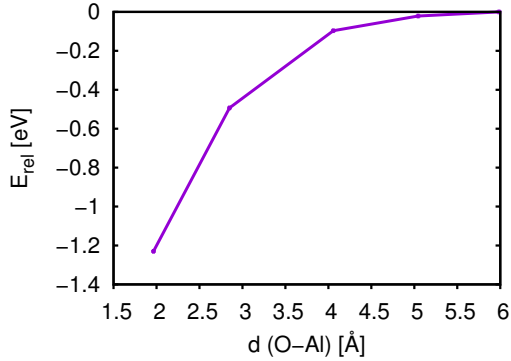


Figure 3.1: Energy profile of the adsorption process, relative to the energy of the system with a distance of 5.98 Å. The $d(\text{O-Al})$ denotes the distance between the oxygen atom of the water and the Al-CUS where the water is/was adsorbed molecularly.

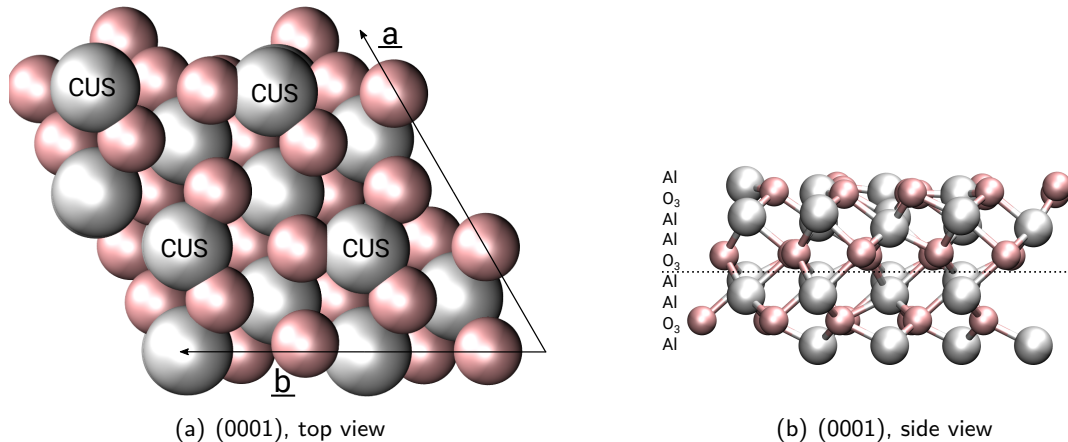


Figure 3.2: Surface model of the (0001), the most stable surface cur under UHV conditions. The top view (a) shows 4 Al CUS atoms, that are surrounded by three threefold coordinated surface oxygen atoms. (b) reveals the Al terminated surface cut in detail with the atomic layers.

3.2 AIMD for MBS Process

Intro, Hass, pinhole dosing vs. molecular beam source (= equilibrium situation vs non-equilibrium) higher dissociation probability, understanding these differences via AIMD. heavy water (D_2O) was used instead of H_2O to better compare with existing MBS experiments by R. K. Campen.

3 Water on $\alpha\text{-Al}_2\text{O}_3(0001)$

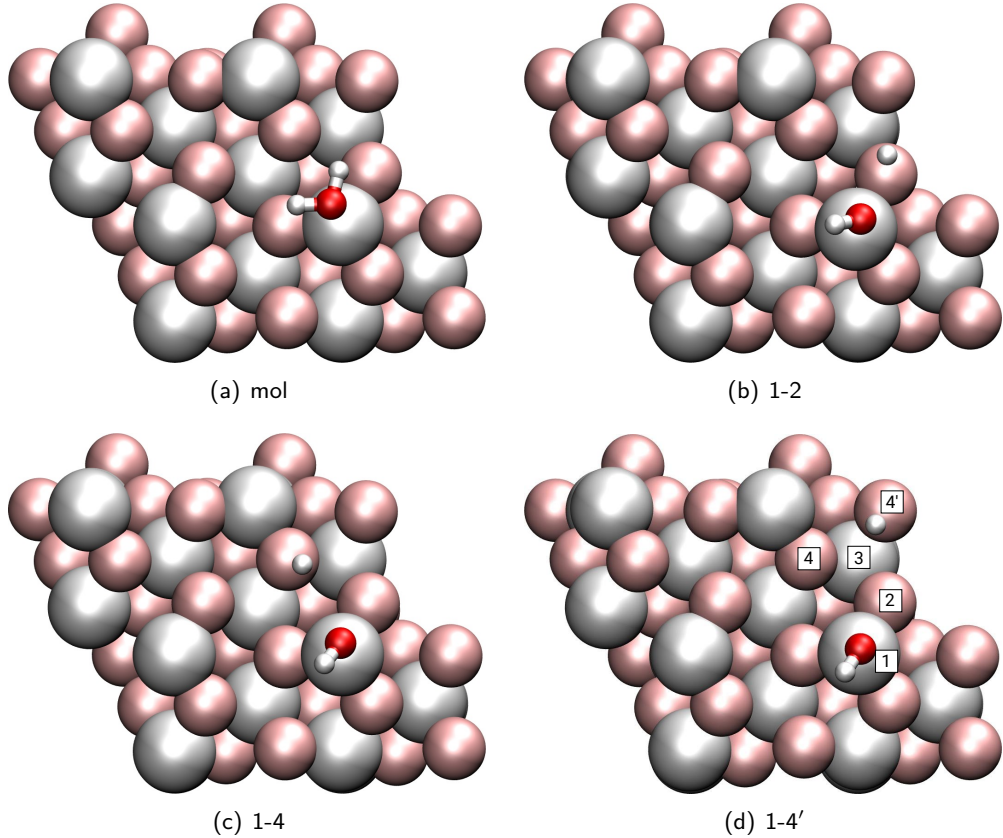


Figure 3.3: Adsorption geometries of the molecular and the three dissociated species. Adsorption energies for these species can be found in Table 3.1.

3.2.1 Beam Model

For the understanding of a Molecular Beam source experiment, the introduction of a beam is an essential part of the model. However, it was not possible to compute a fully realistic beam that was statistically converged, which would require wide knowledge about energy and velocity distributions and a systematic high dimensional sampling, that is not feasible with the computational power available at the moment. Instead as a first approach, a single, rigid water (D₂O) molecule (initial parameters are $d_{OD} = 0.97\text{\AA}$ and bond angle of 104.5°) was sent perpendicularly from a center of mass position from a distance of 4\AA onto the surface, in agreement with the experiment. Having these degrees of freedom excluded, from the 9 degrees of freedom, six are still left (see Figures 3.4, 3.5 and Table 3.2): two for the impact site $[a_0, b_0]$ as it is given relative to the super cell vectors \underline{a} and \underline{b} , three Euler angles α, β and γ for the rotational orientation of the molecule with respect to the surface and the kinetic energy E_{kin} that gives the molecule a momentum towards the surface, solely as translational motion, no

vibration or rotation included. These parameters are varied systematically to gain insight into the process.

As was mentioned before, the barriers can be high (and corresponding rates low), especially for the H-diffusion reactions, but the adsorption process itself is barrierless, and additionally the incoming water molecule has kinetic energy so that processes, that are slow at room temperature otherwise, can be speeded up.

Further improvements of this simplest model are made in subsections 3.2.6 and 3.2.6, that address clustering and rotational and vibrational excited water, respectively. Further details are given there.

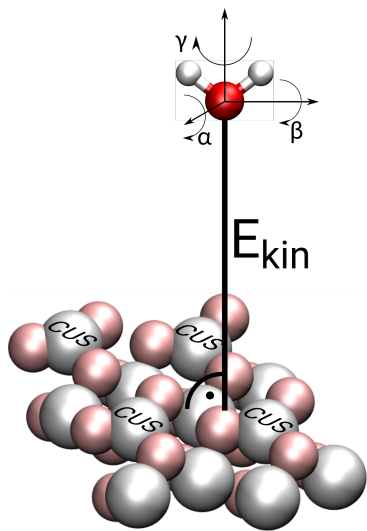


Figure 3.4: Sketch for initial parameters of the trajectories. The water molecule is situated 4 Å above the surface and is arranged within the shown coordinate system, before being shot onto the surface with a defined kinetic energy E_{kin} .

3.2.2 Example Trajectories

Before going to the details, example trajectories for each process leading to one of the four most stable adsorbed species, molecular adsorption, 1-2 dissociation, 1-4 dissociation and 1-4' dissociation are shown in Figure 3.6, the applied parameters are reported in the respective caption. These figures were all obtained from canonical calculations (NVT) at 300 K (see Figure 3.6, the trajectory shown in (d) was additionally preexcited in the asymmetric stretch mode leading to 1-4' dissociation). As one can see, molecular, 1-2 and 1-4 dissociated species can occur directly at the impact time of the water molecule at the surface and is henceforth called direct dissociation from the gas phase. For the 1-4' dissociation shown in Fig. 3.6(d), this process does not happen directly at the impact but (in this case) ca. 40 fs later, so this is referred

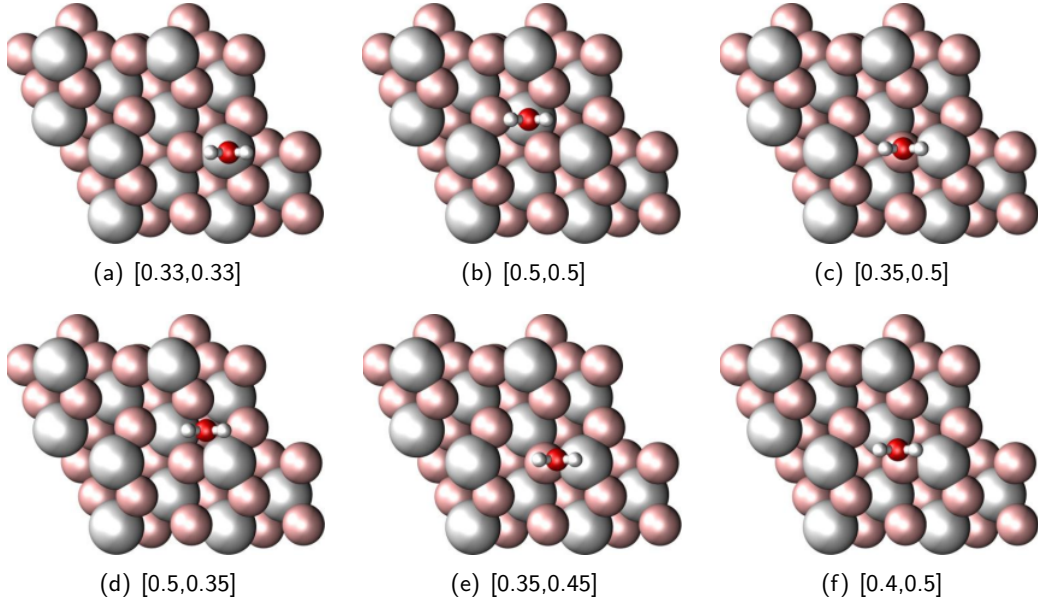


Figure 3.5: The six impact points $[a_0, b_0]$ that were used in the AIMD calculations (shown for the rotational orientation $[0, 0, 0]$, topview).

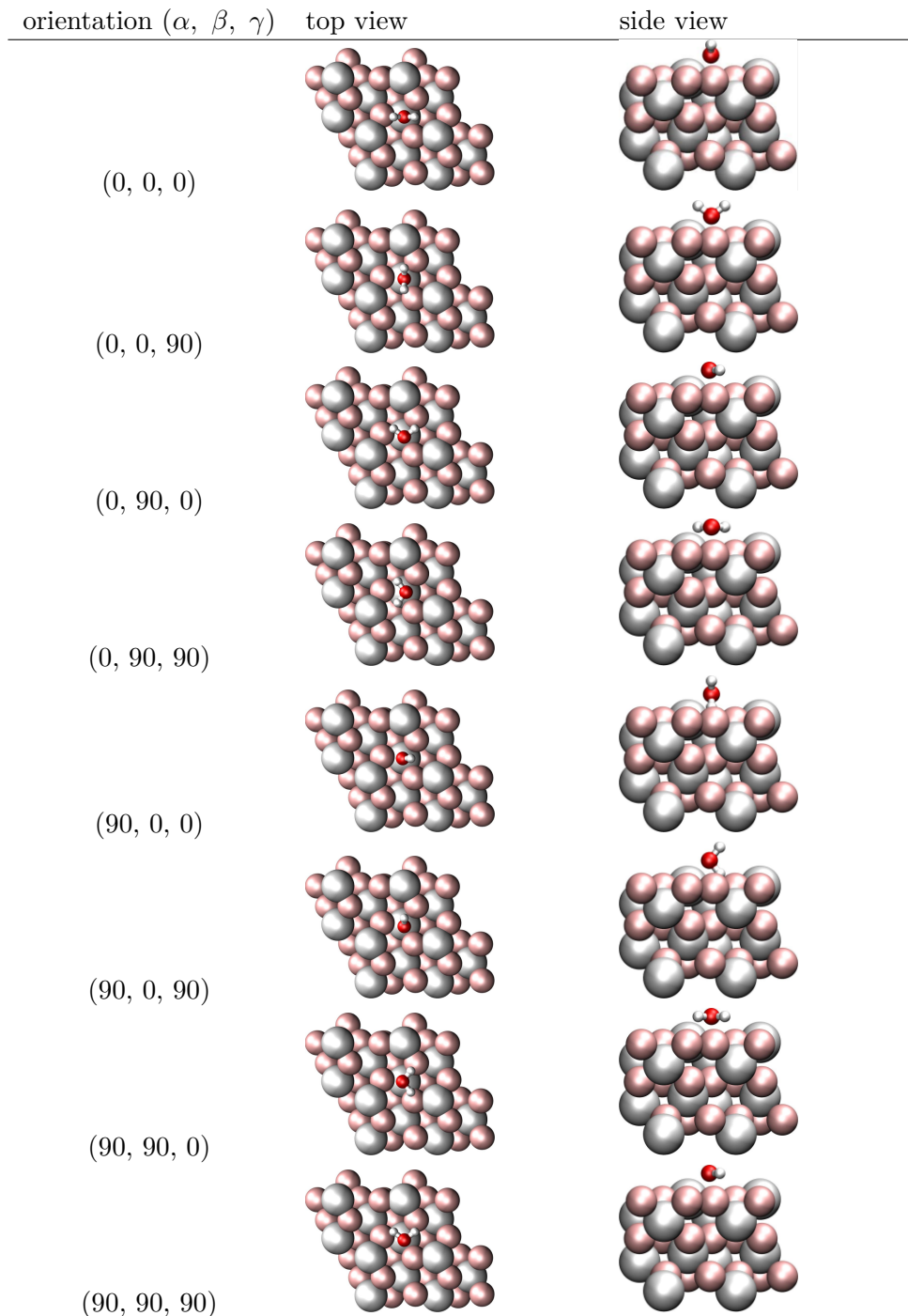
to as indirect dissociation with a molecular intermediate. This indirect process is not unique for the 1-4' dissociated species, all the other species including the molecular can be observed to happen indirectly by either being reflected first from the surface before adsorbing/dissociating or by adsorbing molecularly before dissociating. However, the 1-4' species was the only one that could not be observed after direct dissociation.

3.2.3 Microcanonical AIMD at clean surface

The effects of a single D_2O shot to the cool surface with a NVT ensemble (microcanonical AIMD) were studied systematically by probing over 5 different kinetic energies (from 0.5 to 0.9 eV in 0.1 eV steps), six lateral impact points at the surface ($[0.33, 0.33]$, $[0.5, 0.5]$, $[0.35, 0.5]$, $[0.5, 0.35]$, $[0.35, 0.45]$, $[0.4, 0.5]$, see also Figure 3.5) and eight different orientations of the water with respect to the surface ($[0, 0, 0]$, $[0, 0, 90]$, $[0, 90, 0]$, $[0, 90, 90]$, $[90, 0, 0]$, $[90, 0, 90]$, $[90, 90, 0]$, $[90, 90, 90]$, see also Tab.3.2). These $5 \times 6 \times 8 = 240$ AIMD trajectories for the clean surface at $T = 0\text{ K}$ were carried out for ca 1.2 ps each.

In the trajectories either molecular adsorption, 1-2 dissociation or reflection could be observed. Dissociation was assumed, if the OD distance was greater than 1.3 \AA , but it was made sure that the results did not differ for a greater cutoff distance. Interestingly, only 1-2 dissociation and no 1-4 dissociation could be observed for the conditions (NVT, clean surface), although

Table 3.2: Orientations of the water molecule. Shown are both top view and side view at impact point 0.5,0.5. (look from the right-hand side to the top view)



3 Water on $\alpha\text{-Al}_2\text{O}_3(0001)$

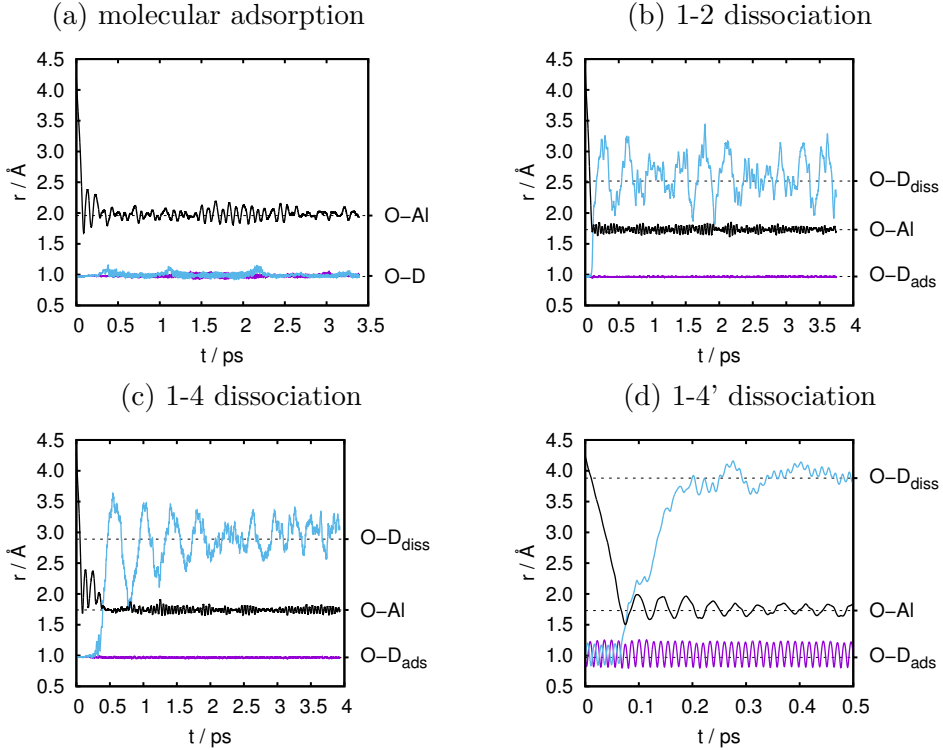


Figure 3.6: Exemplary trajectories for trajectories of different initial parameters, leading to the four adsorption states of water at the $\alpha\text{-Al}_2\text{O}_3(0001)$ surface as indicated in Figs.3.3(a)-(d). For all cases these are canonical (NVT) trajectories at $T = 300$ K. The initial parameters: (a) $E_{\text{kin}} = 0.7$ eV, $[a_0, b_0] = [0.33, 0.33]$, $[\alpha, \beta, \gamma] = [0, 0, 90]$ (in $^\circ$); (b) $E_{\text{kin}} = 0.7$ eV, $[a_0, b_0] = [0.35, 0.45]$, $[\alpha, \beta, \gamma] = [0, 0, 0]$; (c) $E_{\text{kin}} = 0.7$ eV, $[a_0, b_0] = [0.33, 0.33]$, $[\alpha, \beta, \gamma] = [0, 90, 0]$; (d) $E_{\text{kin}} = 0.7$ eV, $[a_0, b_0] = [0.35, 0.5]$, $[\alpha, \beta, \gamma] = [0, 0, 0]$, and the water molecule was vibrationally preexcited along the asymmetric stretch normal coordinate as specified in Subsec. 3.2.6. The r values indicate bond lengths between water-O and the CUS Al atom on which either D_2O or the water hydroxyl unit OD adsorb (O-Al), the distance between water-O and D in non-dissociated (fragments of) D_2O (O-D or O-D_{ads}), and the distance between water-O and D in dissociated (fragments) of D_2O (O-D_{diss}), respectively. The corresponding interatomic distances of the adsorbed species from the static DFT calculations reported in Figs.3.3(a)-(d) are shown as horizontal, dashed lines. In (d), the 1-4' state is reached via a 1-2 dissociation intermediate, which is very short-lived around 0.1 ps.

the molecular and the 1-4 dissociated species are almost equal in energy, and also the barrier heights for the dissociation to 1-2 (0.13 eV) and 1-4 (0.19 eV) do not differ largely. As it is shown later, other conditions are necessary for reaching 1-4 dissociation.

For a statistical analysis of the data see Figure 3.7, where the probabilities for reflection, molecular adsorption and 1-2 dissociation are shown as a function of the kinetic energy (a),

3.2 AIMD for MBS Process

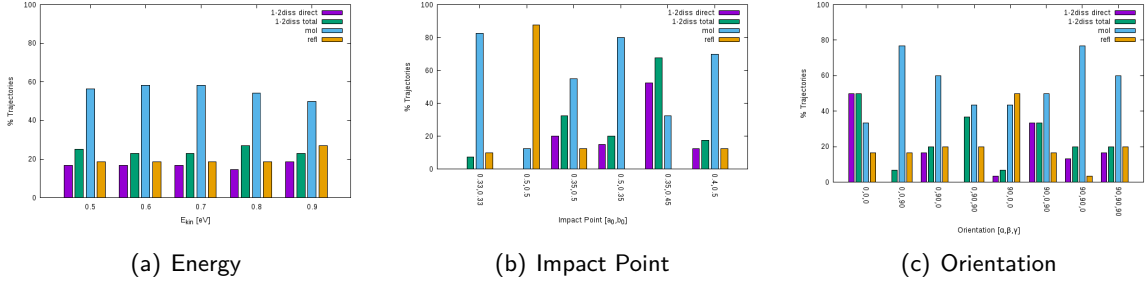


Figure 3.7: Statistics of AIMD trajectories at $T = 0$ (NVE), for single D_2O approaching a clean alumina(0001) surface. In (a), for each of the five different initial kinetic energies E_{kin} , results are averaged over the $6 \times 8 = 48$ combinations of impact sites and rotational orientations. In (b), for each of six different initial impact points $[a_0, b_0]$, results are averaged over $5 \times 8 = 40$ combinations of kinetic energies and rotational orientations. In (c), each of the eight different initial rotational orientations $[\alpha, \beta, \gamma]$, results are averaged over $5 \times 6 = 30$ combinations of kinetic energies and impact points. Columns show percentages of trajectories leading to reflection ("refl"), molecular adsorption ("mol"), and direct and total 1-2 dissociation ("1-2 diss direct" and "1-2 diss total"). (No columns if no trajectories of the type were found.)

impact point (b) and the orientation (c). There also between direct and indirect dissociation is distinguished. Admittedly, this analysis is restricted by the number of trajectories (240). From these figures and the data one can derive the following conclusions:

As anticipated, all three processes could be observed, reflection (20.4%, 49 of the 240 trajectories), molecular adsorption (55.4%, 133 trajectories) and 1-2 dissociation (24.2%, 58 trajectories).

Looking at the impact of the energy in Fig. 3.7(a), the result do not depend largely on the initial kinetic energy of the molecule, at least for the probed energy range. In all cases molecular adsorption dominates, followed by 1-2 dissociation and reflection, that are in the same range around 20-25%. This reflecion probability P_{diss} is only increased for 0.9 eV, at the expense of the molecular species. To tackle the low energy regime, one additional trajectory of 0.1 eV was done ($[a_0, b_0] = [0.35, 0.45]$; $[\alpha, \beta, \gamma] = [0, 0, 0]$), for which $P_{diss} = 1$ for all energies ≥ 0.5 eV. In the case of $E_{kin} = 0.1$ eV, the trajectory only shows molecular adsorption. This result was rather surprising, since the kinetic energy plus the adsorption energy minus the barrier height is with $(0.1 + 1.31 - 0.13)$ eV = .28 eV larger than the reaction barrier. It seems that the excess energy is not available for the OD-bond breaking and instead relaxes in other degrees of freedom of the system. That allows to draw the conclusion, that a minimum kinetic energy is necessary for the dissociation process. In the experiments of R. K. Campen, a kinetic energy of the beam between 0.6 and 0.75 eV is used. This minimum energy constraint can be one possible explanation of the difference between MBS and pinhole dosing. In the latter case, the

3 Water on $\alpha\text{-Al}_2\text{O}_3(0001)$

only energy of a water molecule comes from the thermal energy that is for a D_2O molecule in the gas phase at 300 K around $\frac{3}{2}k_B T \approx 40$ meV.

In contrast to the kinetic energy, the lateral impact point at the surface has a great influence on adsorption and dissociation probabilities (see Fig. 3.7). For the impact point [0.5,0.5], that is at a non-surface Al position, 88% of the trajectories get reflected and molecular adsorption and 1-2 dissociation are oppressed, whereas for [0.33,0.33] that is directly on top of a CUS position, 83% adsorb molecularly and dominates clearly over 1-2 dissociation. In contrast to both sites, [0.35,0.45] which is a gap between an Al CUS position and a neighboring oxygen atom leads to a high dissociation probability of $P_{\text{diss}} \approx 68\%$ with a minor percentage of indirect dissociation. This high dissociation probability can be explained by the fact, that the molecule hits the surface already in a “product-like” geometry, so that the OD bond breakage.

orientation

direct vs indirect

3.2.4 Thermalized Surface

both the 100 trajectories for the 5 parameter sets and the two trajectories for all 6x8 parameters.

3.2.5 Refined Surface Model

precoverage, both 0K and 300K, water was shot in vicinity to preadsorbed D_2O and also around neighboring CUS atom.

3.2.6 Refined Beam Model

Clustering

$(\text{D}_2\text{O})_4$ cluster and also one type of $(\text{D}_2\text{O})_2$ was tested

Rotationally and vibrationally Preexcited Water

excitation, more qualitative.

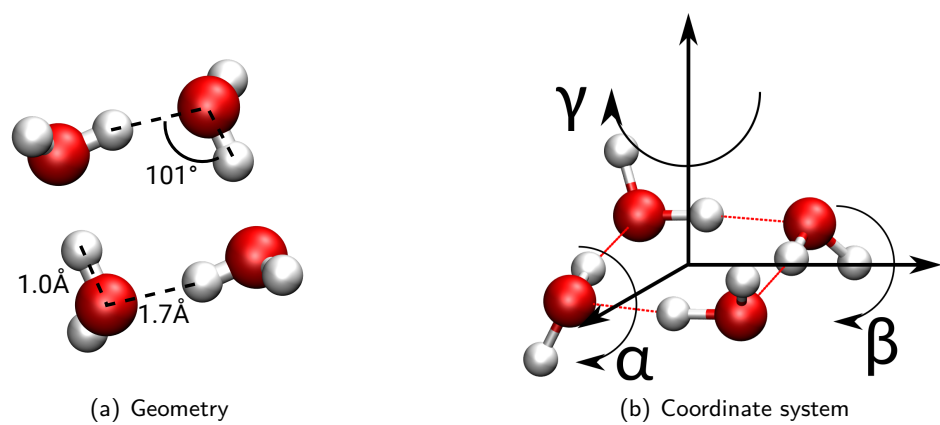


Figure 3.8: $(\text{D}_2\text{O})_4$ cluster for simulation of effects of higher coverages. (a) shows the geometry, especially the DOD bond angle and the OD bond length of neighboring molecules and (b) shows the coordinate system for the rotations along the axes.

3 Water on $\alpha\text{-Al}_2\text{O}_3(0001)$

3.3 Improvement of Reaction Rates

For a model reaction we try to improve the reaction rate with different new methods. This reaction is a H-diffusion reaction on the (0001) surface studied before in our group, the Df-H-4-2 reaction, that moves a proton in the 1-4 position to the OH residue to the 1-2 dissociated state. The rates were before calcualted with PBE+D2/3? and Nudged Elastic Band. An approach were singlepoint calculations were done for the minima and the transition state was also done. For this process also a 1-D potential energy surface was calculated and then the Schrödinger equation was solved to obtain the wave function and see the localization/delocalization of the reaction pathway.

Now we want to expand these methods to the following 3/4/don't know? First we want to calculate the adsorption energies and the barrier within a atom centered orbital method with the hybrid functional B3LYP and also go beyond density functional theory and go to perturbation theory (LMP2).

Apart from that, we study this reaction with the help of Path Integral Molecular Dynamics, where the system is represented as a couple of beads that are connected and henceforth act as a more delocalized particle which can contribute to quantum effects, proton tunneling.

As a last approach, we want to apply other higher level methods in an embedded approach. We cut a cluster from the surface situation and embed this cluster in a field of point charges. By doing this we can calculate the cluster with a better method, let's say B3LYP, CCSD or MP2 and then apply a subtractional scheme to get to corrected adsorption energies that can then be used to improve the rates with Eyring's equation for transtition states.

3.3.1 MP2 and B3LYP

Going beyond pure density functionals and also beyond DFT has been too costly for a long time, simply not applicable for surface adsorbat system that large and electron rich. In the crystal/cryscor code one uses atom centered bases instead of plane waves and so large scale systems can also be computed. We first optimized our parameters with HF calculations and then did calculations with PBE similar to prior plane wave based calculations.

We found out, that BSSE takes a big part, but corrections are not easily applied because the ghosted calculations needed for that do not converge for all the structures with a bigger OH-H distance. Instead we have to use bigger basis sets containing diffuse functions in order to handle the BSSE. Such a self designed basis set by our cooperation partner Dr. Denis Usyat (HU Berlin, group of Martin Schütz) was used here. With this basis set we did the PBE calculations again (?) and the B3LYP as well as the MP2 calculations. First we compared the differences in adsorption energies. We furthermore compared the vibrational frequencies from B3LYP with

3.3 Improvement of Reaction Rates

the ones from VASP/PBE to see a methodological effect.

We also reoptimized the transition state for the Df-H-4-2 reaction.

Not sure if this will come into the diss? No real results obtained..?

3.3.2 PIMD

Instead of examining reactions with a defined reaction pathway as with NEB, we apply the path integral MD to propagate the 1-4 dissociated state in the hope to watch the reaction and to extract from that a time for the reaction (*? it is not really a rate*). But unluckily, no reaction occurred in the given propagation time, so that one only can see the delocalization of the proton. At a given temperature of 300 K the proton only moves a little, far away from any reactive trajectory.

A huge problem was the unit cell: when all atoms or only a few atoms were allowed to move during the trajectory, the whole cell drifted away, as if the periodic boundary conditions would not apply. When fixing all the atoms except for the proton that diffuses it was fine.

cell optimizations were tried, but didn't work as planned; fixing only the rim lead to other atom's movement, maybe one can free the OH group and the Al atom on which the H sits?

We used also PBE but without dispersion corrections and for the trajectories at 300 K we applied the Nosé Hoover thermostat.

3.3.3 QM/QM Embedding Scheme

In order to recalculate adsorption energies and reaction rate constants with a higher level method we tried to apply the mechanical embedding scheme developed in the Sauer group from HU Berlin. One uses a subtractive scheme to correct energies, after calculating the complete system with the low level method (here PBE), the interesting part, namely the cluster, with both the low level method and the high level method (B3LYP, MP2 or CCSD). The high-level:low-level corrected energy is then calculated by the following equation: *equation*

First of all, a reasonable cluster has to be chosen, which is difficult since the 1-4' needs a big cluster to be considered. We chose then the Al₈O₁₂-cluster used in unpublished work from the same group. This cluster was used for tests but when it came to embedding, the Turbomole package failed to compute the embedded system, because hexagonal cells were not yet implemented into the code.

Summary

We made great progress in understanding the $(11\bar{2}0)$ surface of $\alpha\text{-Al}_2\text{O}_3$ in contact with water in the low coverage regime.

The dissociation process of water on (0001) surface was studied.

Several methods were tested to improve reaction rates.

Acknowledgment

I want to thank my doctoral father Prof. Dr. Saalfrank, for giving me the scientific opportunity to research on surface systems and all the valuable discussions and advices. Also I am deeply grateful to my supervisor Dr. Jonas Wirth who gave me support during my time starting as a Bachelor's student, during my Master's thesis and also through the beginning of my PhD, PD Dr. Tillmann Klamroth for discussions about programming and theoretical questions that arose during the work, Dr. Radosław Włodarczyk for his endless knowledge with vasp and programming in general, Giacomo Melani (soon to be Dr.) for his advice and his help, and also the discussions about our teaching duties in mathematics and the whole workgroup for all the valuable discussions and the help. Also for the great atmosphere, that was some times productive and some times also just relaxing and felt very comfortable, here especially Clemens Rietze, Robert Scholz, Gereon Floss, and Steven Lindner. Also I want to thank my second supervisor Beate Paulus for discussion and help beyond research topics. Great acknowledgement to my experimental cooperation partners from FHI, Yanhua Yue, Dr. Harald Kirsch and Dr. Kramer R. Campen for the great work and publications we did together. Thanks to Dr. Denis Usvyat for all his patience and knowledge and valuable discussions about crystal/crysccor and his help. Maristella Alessio from Sauer group (HU Berlin) for help with Turbomole and setting the mechanical embedding calculations, that unluckily did not work for the applied cluster. Ji Chen and Wei Fang from Michaelides group from UCL London for their help with cp2k and i-Pi, necessary for the PIMD calculations. Last I want to thank Dr. Jean Christophe Tremblay who brought me to theoretical chemistry by bringing my attention to this field of science. Christiane Wunderlich who was my school teacher in chemistry, without whom I would not have studied chemistry.

Appendix

reaction pathways: dissociationCb-iCa2 and Cb-iCb2?

Appendix

Publications

This Work:

- (1) Heiden, S.; Yue, Y.; Kirsch, H.; Wirth, J.; Saalfrank, P.; Campen, R. K.: »Water Dissociative Adsorption on $\alpha\text{-Al}_2\text{O}_3(11\bar{2}0)$ Is Controlled by Surface Site Undercoordination, Density, and Topology«, *Journal of Physical Chemistry C* **2018**, vol, pp.
- (2) Heiden, S.; Wirth, J.; Saalfrank, P.: »Water Molecular Beam Scattering at $\alpha\text{-Al}_2\text{O}_3(0001)$: An *Ab Initio* Molecular Dynamics Study«, *Journal* **2018**, vol, pp.

References

References

Erklärung

Hiermit versichere ich, dass die vorliegende Arbeit an keiner anderen Hochschule eingereicht sowie selbständig und ausschließlich mit den angegebenen Mitteln angefertigt worden ist.

Potsdam, xx 2018